


# TECH BRIEFS

NATIONAL AERONAUTICS AND SPACE ADMINISTRATION

-  **Technology Focus**
-  **Electronics/Computers**
-  **Software**
-  **Materials**
-  **Mechanics/Machinery**
-  **Manufacturing**
-  **Bio-Medical**
-  **Physical Sciences**
-  **Information Sciences**
-  **Books and Reports**
-  **Green Design**



## INTRODUCTION

Tech Briefs are short announcements of innovations originating from research and development activities of the National Aeronautics and Space Administration. They emphasize information considered likely to be transferable across industrial, regional, or disciplinary lines and are issued to encourage commercial application.

### Availability of NASA Tech Briefs and TSPs

Requests for individual Tech Briefs or for Technical Support Packages (TSPs) announced herein should be addressed to

#### National Technology Transfer Center

Telephone No. (800) 678-6882 or via World Wide Web at [www.nttc.edu](http://www.nttc.edu)

Please reference the control numbers appearing at the end of each Tech Brief. Information on NASA's Innovative Partnerships Program (IPP), its documents, and services is also available at the same facility or on the World Wide Web at <http://www.nasa.gov/offices/ipp/network/index.html>

Innovative Partnerships Offices are located at NASA field centers to provide technology-transfer access to industrial users. Inquiries can be made by contacting NASA field centers listed below.

## NASA Field Centers and Program Offices

#### Ames Research Center

Lisa L. Lockyer  
(650) 604-1754  
[lisa.l.lockyer@nasa.gov](mailto:lisa.l.lockyer@nasa.gov)

#### Dryden Flight Research Center

Gregory Poteat  
(661) 276-3872  
[greg.poteat@dfrc.nasa.gov](mailto:greg.poteat@dfrc.nasa.gov)

#### Glenn Research Center

Kathy Needham  
(216) 433-2802  
[kathleen.k.needham@nasa.gov](mailto:kathleen.k.needham@nasa.gov)

#### Goddard Space Flight Center

Nona Cheeks  
(301) 286-5810  
[nona.k.cheeks@nasa.gov](mailto:nona.k.cheeks@nasa.gov)

#### Jet Propulsion Laboratory

Andrew Gray  
(818) 354-3821  
[gray@jpl.nasa.gov](mailto:gray@jpl.nasa.gov)

#### Johnson Space Center

information  
(281) 483-3809  
[jsc.techtran@mail.nasa.gov](mailto:jsc.techtran@mail.nasa.gov)

#### Kennedy Space Center

David R. Makufka  
(321) 867-6227  
[david.r.makufka@nasa.gov](mailto:david.r.makufka@nasa.gov)

#### Langley Research Center

Brian Beaton  
(757) 864-2192  
[brian.f.beaton@nasa.gov](mailto:brian.f.beaton@nasa.gov)

#### Marshall Space Flight Center

Jim Dowdy  
(256) 544-7604  
[jim.dowdy@msfc.nasa.gov](mailto:jim.dowdy@msfc.nasa.gov)

#### Stennis Space Center

Ramona Travis  
(228) 688-3832  
[ramona.e.travis@nasa.gov](mailto:ramona.e.travis@nasa.gov)

#### Carl Ray, Program Executive

Small Business Innovation  
Research (SBIR) & Small  
Business Technology  
Transfer (STTR) Programs  
(202) 358-4652  
[carl.g.ray@nasa.gov](mailto:carl.g.ray@nasa.gov)

#### Doug Comstock, Director

Innovative Partnerships  
Program Office  
(202) 358-2560  
[doug.comstock@nasa.gov](mailto:doug.comstock@nasa.gov)





# TECH BRIEFS

NATIONAL AERONAUTICS AND SPACE ADMINISTRATION



## 5 Technology Focus: Sensors

- 5 Cryogenic Flow Sensor
- 5 Multi-Sensor Mud Detection
- 6 Gas Flow Detection System
- 6 Mapping Capacitive Coupling Among Pixels in a Sensor Array
- 7 Fiber-Based Laser Transmitter for Oxygen A-Band Spectroscopy and Remote Sensing
- 7 Low-Profile, Dual-Wavelength, Dual-Polarized Antenna
- 8 Time-Separating Heating and Sensor Functions of Thermistors in Precision Thermal Control Applications



## 9 Electronics/Computers

- 9 Cellular Reflectarray Antenna
- 10 A One-Dimensional Synthetic-Aperture Microwave Radiometer
- 10 Electrical Switching of Perovskite Thin-Film Resistors
- 11 Two-Dimensional Synthetic-Aperture Radiometer
- 11 Ethernet-Enabled Power and Communication Module for Embedded Processors
- 12 Electrically Variable Resistive Memory Devices



## 13 Manufacturing & Prototyping

- 13 Improved Attachment in a Hybrid Inflatable Pressure Vessel
- 14 Electrostatic Separator for Beneficiation of Lunar Soil



## 15 Mechanics/Machinery

- 15 Amorphous Rover
- 16 Space-Frame Antenna
- 17 Gear-Driven Turnbuckle Actuator
- 17 *In-Situ* Focusing Inside a Thermal Vacuum Chamber
- 18 Space-Frame Lunar Lander



## 21 Materials

- 21 Wider-Opening Dewar Flasks for Cryogenic Storage
- 21 Silicon Oxycarbide Aerogels for High-Temperature Thermal Insulation

21 Supercapacitor Electrolyte Solvents With Liquid Range Below  $-80^{\circ}\text{C}$

22 Designs and Materials for Better Coronagraph Occulting Masks



## 23 Green Design

- 23 Fuel-Cell-Powered Vehicle With Hybrid Power Management
- 24 Fine-Water-Mist Multiple-Orientation-Discharge Fire Extinguisher
- 25 Fuel-Cell Water Separator



## 27 Physical Science

- 27 Turbulence and the Stabilization Principle
- 27 Improved Cloud Condensation Nucleus Spectrometer
- 28 Better Modeling of Electrostatic Discharge in an Insulator
- 29 Sub-Aperture Interferometers
- 30 Terahertz Mapping of Microstructure and Thickness Variations
- 31 Multiparallel Three-Dimensional Optical Microscopy
- 31 Stabilization of Phase of a Sinusoidal Signal Transmitted Over Optical Fiber
- 33 Vacuum-Compatible Wideband White Light and Laser Combiner Source System
- 33 Optical Tapers as White-Light WGM Resonators
- 34 EPR Imaging at a Few Megahertz Using SQUID Detectors
- 35 Reducing Field Distortion in Magnetic Resonance Imaging



## 37 Bio-Medical

- 37 Fluorogenic Cell-Based Biosensors for Monitoring Microbes
- 37 A Constant-Force Resistive Exercise Unit
- 37 GUI To Facilitate Research on Biological Damage From Radiation
- 38 On-Demand Urine Analyzer
- 38 More-Realistic Digital Modeling of a Human Body
- 38 Advanced Liquid-Cooling Garment Using Highly Thermally Conductive Sheets

This document was prepared under the sponsorship of the National Aeronautics and Space Administration. Neither the United States Government nor any person acting on behalf of the United States Government assumes any liability resulting from the use of the information contained in this document, or warrants that such use will be free from privately owned rights.





## Cryogenic Flow Sensor

*Marshall Space Flight Center, Alabama*

An acousto-optic cryogenic flow sensor (CFS) determines mass flow of cryogens for spacecraft propellant management. The CFS operates unobtrusively in a high-pressure, high-flow-rate cryogenic environment to provide measurements for fluid quality as well as mass flow rate. Experimental hardware uses an optical “plane-of-light” (POL) to detect the onset of two-phase flow, and the presence of particles in the flow of water.

Acousto-optic devices are used in laser equipment for electronic control of the intensity and position of the laser beam. Acousto-optic interaction occurs in all optical media when an acoustic

wave and a laser beam are present. When an acoustic wave is launched into the optical medium, it generates a refractive index wave that behaves like a sinusoidal grating. An incident laser beam passing through this grating will diffract the laser beam into several orders. Its angular position is linearly proportional to the acoustic frequency, so that the higher the frequency, the larger the diffracted angle.

If the acoustic wave is traveling in a moving fluid, the fluid velocity will affect the frequency of the traveling wave, relative to a stationary sensor. This frequency shift changes the angle of diffraction, hence, fluid velocity can be de-

termined from the diffraction angle. The CFS acoustic Bragg grating data test indicates that it is capable of accurately determining flow from 0 to 10 meters per second. The same sensor can be used in flow velocities exceeding 100 m/s. The POL module has successfully determined the onset of two-phase flow, and can distinguish vapor bubbles from debris.

*This work was done by John Justak of Advanced Technologies Group, Inc. for Marshall Space Flight Center. For more information, contact Sammy Nabors, MSFC Commercialization Assistance Lead, at [sammy.a.nabors@nasa.gov](mailto:sammy.a.nabors@nasa.gov). Refer to MFS-32730-1.*

## Multi-Sensor Mud Detection

**This technology is also applicable to terrain hazard assessment in terrestrial or planetary situations.**

*NASA's Jet Propulsion Laboratory, Pasadena, California*

Robust mud detection is a critical perception requirement for Unmanned Ground Vehicle (UGV) autonomous off-road navigation. A military UGV stuck in a



A General Dynamics Robotic Systems (GDRS) experimental unmanned vehicle (XUV) navigates through a muddy grass field during a data collection for the **Daytime Mud Detection System**.

mud body during a mission may have to be sacrificed or rescued, both of which are unattractive options. There are several characteristics of mud that may be detectable with appropriate UGV-mounted sensors. For example, mud only occurs on the ground surface, is cooler than surrounding dry soil during the daytime under nominal weather conditions, is generally darker than surrounding dry soil in visible imagery, and is highly polarized. However, none of these cues are definitive on their own. Dry soil also occurs on the ground surface, shadows, snow, ice, and water can also be cooler than surrounding dry soil, shadows are also darker than surrounding dry soil in visible imagery, and cars, water, and some vegetation are also highly polarized. Shadows, snow, ice, water, cars, and vegetation can all be disambiguated from mud by using a suite of sensors that span multiple bands in the electromagnetic spectrum. Because there are military operations when it is imperative for UGV's to operate without emitting strong, de-

tectable electromagnetic signals, passive sensors are desirable.

JPL has developed a daytime mud detection capability using multiple passive imaging sensors. Cues for mud from multiple passive imaging sensors are fused into a single mud detection image using a rule base, and the resultant mud detection is localized in a terrain map using range data generated from a stereo pair of color cameras. Thus far at the time of this reporting, JPL has:

1. Performed daytime data collections, on wet and dry soil, with several candidate passive imaging sensors, including multi-spectral (blue, green, red, and near-infrared bands), short-wave infrared, mid-wave infrared, long-wave infrared, polarization, and a stereo pair of color cameras.
2. Characterized the advantages and disadvantages of each passive imaging sensor to provide cues for mud.
3. Implemented a first-generation mud detector that uses a stereo pair of color

cameras and a polarization camera. For each set of input images, the innovators calculate degree of linear polarization (DOLP), back-project polarization pixels that have high DOLP into the left color image, generate a stereo range image (which is registered with the left color image), and insert detected mud into a world map using the stereo range data. As it is only expected for mud to occur on the ground surface, stereo range data are used to isolate ground surface pixels from the other pixels corresponding to ground clutter. Ground

clutter pixels with high DOLP (such as vegetation) are ignored.

Techniques to estimate soil moisture content have been studied for decades for agricultural applications; however, mud detection for UGV autonomous navigation is a relatively new research area. Ground vehicle methods of soil moisture estimation have used passive microwave sensors, but the antennas tend to be bulky and have been mounted directly downwards. This requires a UGV to drive on potentially hazardous terrain in order to characterize it. This work involves de-

tecting mud hazards from a UGV without having to drive on the hazard first.

Mud detection is a terrestrial application; however, the intermediate image processing steps and world modeling techniques performed for this task are valuable to terrain hazard assessment in general, terrestrial, or planetary situations.

*This work was done by Arturo L. Rankin and Larry H. Matthies of Caltech for NASA's Jet Propulsion Laboratory. For more information, contact [iaoffice@jpl.nasa.gov](mailto:iaoffice@jpl.nasa.gov). NPO-46624*

---

## Gas Flow Detection System

**Commercial applications include flow measurement systems.**

*John F. Kennedy Space Center, Florida*

This system provides a portable means to detect gas flow through a thin-walled tube without breaking into the tubing system. The flow detection system was specifically designed to detect flow through two parallel branches of a manifold with only one inlet and outlet, and is a means for verifying a space shuttle program requirement that saves time and reduces the risk of flight hardware damage compared to the current means of requirement verification.

The prototype Purge Vent and Drain Window Cavity Conditioning System (PVD WCCS) Flow Detection System consists of a heater and a temperature-sensing thermistor attached to a piece of Velcro to be attached to each branch of a WCCS manifold for the duration of the requirement verification test. The heaters and thermistors are connected to a shielded cable and then to an electronics enclosure, which contains the power supplies, relays, and circuit board to provide power, signal conditioning, and control. The electronics enclosure is then connected to a commercial data acquisition box to provide analog to

digital conversion as well as digital control. This data acquisition box is then connected to a commercial laptop running a custom application created using National Instruments' LabVIEW.

The operation of the PVD WCCS Flow Detection System consists of first attaching a heater/thermistor assembly to each of the two branches of one manifold while there is no flow through the manifold. Next, the software application running on the laptop is used to turn on the heaters and to monitor the manifold branch temperatures. When the system has reached thermal equilibrium, the software application's graphical user interface (GUI) will indicate that the branch temperatures are stable. The operator can then physically open the flow control valve to initiate the test flow of gaseous nitrogen (GN<sub>2</sub>) through the manifold. Next, the software user interface will be monitored for stable temperature indications when the system is again at thermal equilibrium with the test flow of GN<sub>2</sub>. The temperature drop of each branch from its "no flow" stable

temperature peak to its stable "with flow" temperature will allow the operator to determine whether a minimum level of flow exists.

An alternative operation has the operator turning on the software only long enough to record the ambient temperature of the tubing before turning on the heaters and initiating GN<sub>2</sub> flow. The stable temperature of the heated tubing with GN<sub>2</sub> flow is then compared with the ambient tubing temperature to determine if flow is present in each branch. To help quantify the level of flow in the manifolds, each branch will be bench calibrated to establish its thermal properties using the flow detection system and different flow rates. These calibration values can then be incorporated into the software application to provide more detailed flow rate information.

*This work was done by Thomas Moss, Curtis Ihlefeld, and Barry Slack of Kennedy Space Center. For further information, contact the Kennedy Applied Physics Laboratory at (321) 867-7513. KSC-13174*

---

## Mapping Capacitive Coupling Among Pixels in a Sensor Array

**Cross-talk calibration of all pixels can be performed efficiently.**

*NASA's Jet Propulsion Laboratory, Pasadena, California*

An improved method of mapping the capacitive contribution to cross-talk among pixels in an imaging array of sensors (typically, an imaging photodetector array) has been devised for use in calibrating and/or

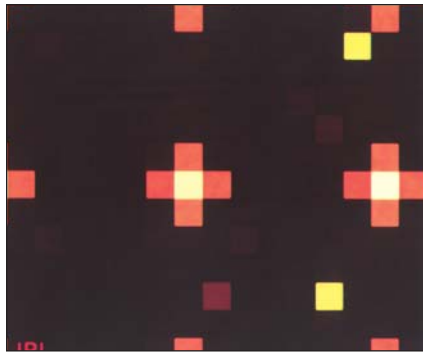
characterizing such an array. The method is applicable to almost all image detectors in modern electronic cameras for diverse applications, ranging from consumer cellular-telephone cameras at one extreme to

high-performance imaging scientific instruments at the other extreme. In comparison with prior methods of quantifying the capacitive coupling among pixels, this method is a more efficient means of ob-



taining detailed information pertaining to all the pixels. Unlike the prior methods, this method does not require flat-field illumination of the array: indeed, the method does not require any illumination.

The method involves a sequence of resets of subarrays of pixels to specified voltages and measurement of the voltage responses of neighboring non-reset pixels. The spacing of the reset pixels is chosen in accordance with the number of neighboring pixels over which the coupling coefficients are sought. The sequence begins with reset of all the pixels in the array to a specified first voltage level. In the next step, a subarray of pixels is reset to a specified second voltage level. Signals consisting of portions of the second reset voltage change are coupled capacitively from the pixels of the reset subarray to adjacent non-second-reset pixels. These signals can be mapped in the form of difference im-



This **Difference Image** from a portion of an image detector containing a rectangular pixel array was generated from two images: one recorded immediately after and one recorded immediately before the second reset. The second-reset pixels were those residing at intersections of rows and columns at seven-pixel intervals.

ages from the pixel voltages measured immediately before and immediately after the second reset (see figure). The

sequence as described thus far can be repeated for different subarrays of pixels, as needed, to acquire data for characterizing all pixels of interest. The entire sequence can be repeated to acquire multiple sets of data that can be combined to reduce measurement noise.

*This work was done by Suresh Seshadri, David M. Cole, and Roger M. Smith of Caltech for NASA's Jet Propulsion Laboratory.*

*In accordance with Public Law 96-517, the contractor has elected to retain title to this invention. Inquiries concerning rights for its commercial use should be addressed to:*

*Innovative Technology Assets Management  
JPL*

*Mail Stop 202-233*

*4800 Oak Grove Drive*

*Pasadena, CA 91109-8099*

*E-mail: iaoffice@jpl.nasa.gov*

*Refer to NPO-45223, volume and number of this NASA Tech Briefs issue, and the page number.*

## **Fiber-Based Laser Transmitter for Oxygen A-Band Spectroscopy and Remote Sensing**

*Goddard Space Flight Center, Greenbelt, Maryland*

A fiber-based laser transmitter has been designed for active remote-sensing spectroscopy. The transmitter uses a master-oscillator-power-amplifier (MOPA) configuration with a distributed feedback diode-laser master oscillator and an erbium-doped fiber amplifier. The output from the MOPA is frequency-doubled with a periodically poled nonlinear crystal. The utility of this single-frequency, wavelength-tunable, power-scalable laser has been demonstrated in a spectroscopic measurement of the diatomic oxygen A-band.

The problem that needed to be addressed was how to measure atmospheric state parameters (like temperature and pressure) from space to get local measurements and global coverage. The only successful laser transmitter that had been used for this type of measurement (remote sensing from an airplane) used dye and alexandrite lasers. These devices were both spectroscopically and mechanically unstable and very inefficient. This transmitter design offers many advantages over this technology.

Fiber-based technology vastly improves mechanical alignment issues because optical path is inside a waveguide that is spliced together and no longer contingent on the relative alignment of bulk optical parts. Many of the components are built to telecommunications industry reliability standards.

*This work was done by Mark A. Stephen and James B. Abshire of Goddard Space Flight Center. For further information, contact the Goddard Innovative Partnerships Office at (301) 286-5810. GSC-15710-1*

## **Low-Profile, Dual-Wavelength, Dual-Polarized Antenna**

**This antenna system has uses in remote monitoring of ocean storms and in search and rescue operations.**

*Goddard Space Flight Center, Greenbelt, Maryland*

A single-aperture, low-profile antenna design has been developed that supports dual-polarization and simultaneous operation at two wavelengths. It realizes multiple beams in the elevation plane, and supports radiometric, radar, and conical scanning applications.

This antenna consists of multiple azimuth sticks, with each stick being a multilayer, hybrid design. Each stick forms the h-plane pattern of the C and Ku-band vertically and horizontally polarized antenna beams. By combining several azimuth sticks together, the ele-

vation beam is formed. With a separate transceiver for each stick, the transmit phase and amplitude of each stick can be controlled to synthesize a beam at a specific incidence angle and to realize a particular side-lobe pattern. By changing the transmit phase distribution

through the transceivers, the transmit antenna beam can be steered to different incidence angles. By controlling the amplitude distribution, different side-lobe patterns and efficiencies can be realized. The receive beams are formed using digital beam synthesis techniques, resulting in very little loss in the receive path, thus enabling a very-low-loss receive antenna to support passive measurements.

Each azimuth stick consists of a dual-polarized Ku-band slotted waveguide linear array that is one-half of a Ku-band wavelength wide and is center-fed. The latter ensures that grating lobes will not be produced in the full array. The linear array has two sections, one supporting broadside slots and the other "edge" slots. For the broadside slots, a ridge waveguide is used to reduce the width of the waveguide section well below one-half wavelength.

For the initial instrument design, the full array will implement phase steering

to form the transmit beam and digital beam synthesis to form the receive beam. The phase and amplitude of the transmit signal delivered to each vertically and horizontally polarized C and Ku-band port on the array will be controlled through dedicated, phase-locked transceivers. The array will be conically scanned to map a large surface swath beneath the aircraft and provide multiple looks at each along and cross track pixel within the swath. This will permit ocean vector wind scatterometry techniques to be applied. The coincident passive measurements obtained with this antenna will allow the atmospheric attenuation to be estimated and used to aid the ocean vector wind retrieval process, especially in the presence of precipitation where the Ku-band receive signals will be attenuated.

This antenna's compact design will reduce deployment costs for ground-based applications, and will be ideal for mobile applications where space is

often limited. Its ability to separate transmit and receive modes permits very low losses to be achieved during the receive phase, allowing for coincident active and passive measurements. Its flexibility to support frequency, phase, and digital beam synthesis techniques allows it to service a broad market, and its scalability will enable it to be customized to commercial applications at very little cost.

This system has application in monitoring the ocean surface vector wind in tropical cyclones and other severe ocean storms. In defense applications, it has uses where an imaging and mapping dual-band, dual-polarized antenna would provide strategic advantages. Search and rescue missions also can benefit from this antenna technology.

*This work was done by James R. Carswell of Remote Sensing Solutions, Inc. for Goddard Space Flight Center. Further information is contained in a TSP (see page 1). GSC-15706-1*

---

## Time-Separating Heating and Sensor Functions of Thermistors in Precision Thermal Control Applications

**This technology can be applied to telescope sensor and optics uses.**

*NASA's Jet Propulsion Laboratory, Pasadena, California*

A method allows combining the functions of a heater and a thermometer in a single device, a thermistor, with minimal temperature read errors. Because thermistors typically have a much smaller thermal mass than the objects they monitor, the thermal time to equilibrate the thermometer to the temperature of the object ( $\tau_t$ ) is typically much shorter than the thermal time of the object to change its temperature in response to an external perturbation ( $\tau_o$ ),  $\tau_t \ll \tau_o$ .

It is possible to switch the heater controlling the object's temperature off for this shorter length of time. While the heater is switched off, the thermistor is allowed the time equal to several  $\tau_t$  to reach equilibrium with the object, then its temperature is measured, after

which the heater is turned back on. The measured value is provided for any temperature control, and the voltage on the thermistor during the heating portion of the cycle will be determined by that control.

In one tested implementation, the  $\tau_t$  was measured to be under 0.5 ms, and  $\tau_o \approx 2$  s. In the timing sequence in this implementation, the heater circuit is turned off, and the measurement current is turned on. After  $\approx 3$  ms, the voltage readout is accomplished in  $\approx 1$  ms. A fraction of ms later, the heater is turned back on for  $\approx 95$  ms.

In one embodiment of this solution, a sample and hold circuit captures the voltage (resistance) readout during the short measurement interval and provides the capture value for the du-

ration of the cycle. This embodiment can be used with any temperature controller, including off-the-shelf PID controllers.

Another embodiment involves a readout that is synchronized with the multiplexed readout of one sensor in a collection, and the heater is connected to the same sensor while the multiplexer is reading other sensors. This solution requires a PID circuit compatible with the multiplexed readout, typically implemented in an FPGA solution with a clock-driven timing.

*This work was done by Hyung J. Cho, Kalyani G. Sukhatme, John C. Mahoney, Konstantin Penanen, and Rudolph Vargas, Jr., of Caltech for NASA's Jet Propulsion Laboratory. Further information is contained in a TSP (see page 1). NPO-46900*



## Cellular Reflectarray Antenna

**This next-generation antenna has application in the broadband satellite communications market, including conventional or HDTV programming.**

*John H. Glenn Research Center, Cleveland, Ohio*

The cellular reflectarray antenna is intended to replace conventional parabolic reflectors that must be physically aligned with a particular satellite in geostationary orbit. These arrays are designed for specified geographical locations, defined by latitude and longitude, each called a "cell." A particular cell occupies nominally 1,500 mi<sup>2</sup> (3,885 km<sup>2</sup>), but this varies according to latitude and longitude. The cellular reflectarray antenna designed for a particular cell is simply positioned to align with magnetic North, and the antenna surface is level (parallel to the ground). A given cellular reflectarray antenna will not operate in any other cell. There is no need for a

highly skilled installer to mechanically point the antenna. The antenna also has an inherent measure of security (i.e., prevents equipment piracy) because it will not operate outside of its designed cell space.

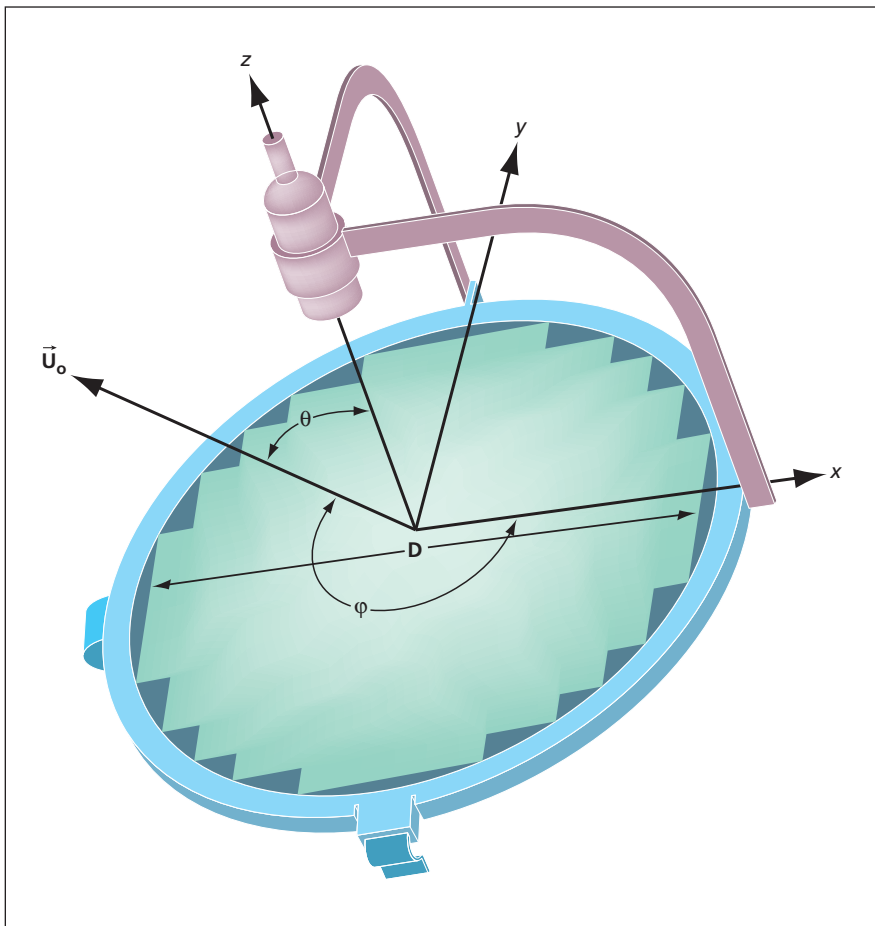
This innovation is more aesthetically pleasing than parabolic reflectors, can be installed by a typical consumer, and is flat so that wind loading is no longer an issue. A software code accepts a subscriber's zip code as input and automatically generates the appropriate phase shifter settings of each reflectarray elemental radiator so that the antenna beam is directed to the appropriate satellite for that subscriber's geographic location.

A given antenna is supplied to a subscriber with an index indicating how to align it to magnetic North. The subscriber simply needs to determine the direction of magnetic North from his or her location. Transmission lines integrated with the elemental radiators are used to induce circular polarization and to provide the proper electrical delay to achieve the required phase shift for that element to contribute effectively to forming a collimated antenna beam in the direction of the geostationary satellite. If transmission lines are affixed to orthogonal edges of an elemental radiator, and one line is electrically 90° longer than the other, the reflected signal from the feed will be polarized in the same sense as the feed. The signal scattered from the elemental radiators and ground plane will be oppositely polarized by virtue of the reversal of propagation direction.

If the dielectric constant and thickness of the printed circuit board substrate are chosen such that the path length difference between the front (elemental radiator) surface and back (ground plane) surface are about 90°, the image from the feed that is projected normal to the array is largely cancelled. By judiciously choosing the substrate thickness and dielectric constant, the reflectarray aperture can operate at two distinct frequencies to cover receive and transmit modes. Using a relatively high dielectric constant material (e.g.,  $\epsilon_r \approx 10$ ) allows interlacing of the low band and high band elements while preserving necessary, half-wavelength inter-element spacing to prevent grating lobes (i.e., to ensure only one main antenna beam).

*This work was done by Robert R. Romanofsky of Glenn Research Center. Further information is contained in a TSP (see page 1).*

*Inquiries concerning rights for the commercial use of this invention should be addressed to NASA Glenn Research Center, Innovative Partnerships Office, Attn: Steve Fedor, Mail Stop 4-8, 21000 Brookpark Road, Cleveland, Ohio 44135. Refer to LEW-18248-1.*



The basic Cellular Reflectarray Platform configuration is shown. The x-axis is aligned to magnetic North, and the z-axis is perpendicular to the ground.

## A One-Dimensional Synthetic-Aperture Microwave Radiometer

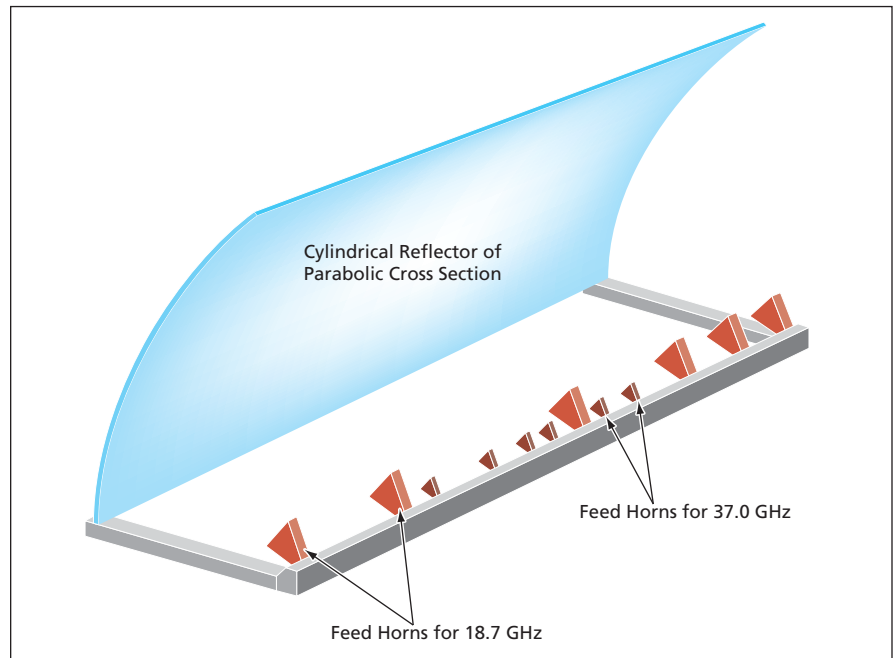
Phased microwave feed horns would be arrayed sparsely along a cylindrical parabolic reflector.

*Goddard Space Flight Center, Greenbelt, Maryland*

A proposed one-dimensional synthetic-aperture microwave radiometer could serve as an alternative to either the two-dimensional synthetic-aperture radiometer described in the immediately preceding article or to a prior one-dimensional one, denoted the Electrically Scanned Thinned Array Radiometer (ESTAR), mentioned in that article. The proposed radiometer would operate in a “push-broom” imaging mode, utilizing (1) interferometric cross-track scanning to obtain cross-track resolution and (2) the focusing property of a reflector for along-track resolution.

The most novel aspect of the proposed system would be the antenna (see figure), which would include a cylindrical reflector of offset parabolic cross section. The reflector could be made of a lightweight, flexible material amenable to stowage and deployment. Other than a stowage/deployment mechanism, the antenna would not include moving parts, and cross-track scanning would not entail mechanical rotation of the antenna. During operation, the focal line, parallel to the cylindrical axis, would be oriented in the cross-track direction, so that placement of receiving/radiating elements at the focal line would afford the desired along-track resolution.

The elements would be microwave feed horns sparsely arrayed along the focal line. The feed horns would be ori-



The **Antenna of the Proposed Radiometer** would consist of microwave feed horns positioned along the focal line of a cylindrical parabolic reflector. In one potential application, there would be two sets of feed horns for operation at two frequencies: the larger ones would be 18.7 GHz, the smaller ones for 37.0 GHz.

ented with their short and long cross-sectional dimensions parallel and perpendicular, respectively, to the cylindrical axis to obtain fan-shaped beams having their broad and narrow cross-sectional dimensions parallel and perpendicular, respectively, to the cylindrical axis. The interference among the beams

would be controlled in the same manner as in the ESTAR to obtain along-cylindrical-axis (cross-track) resolution and cross-track scanning.

*This work was done by Terence Doiron and Jeffrey Piepmeier of Goddard Space Flight Center. Further information is contained in a TSP (see page 1). GSC-14748-1*

## Electrical Switching of Perovskite Thin-Film Resistors

Physical properties are altered in useful ways by applying electrical pulses.

*Marshall Space Flight Center, Alabama*

Electronic devices that exploit electrical switching of physical properties of thin films of perovskite materials (especially colossal magnetoresistive materials) have been invented. Unlike some related prior devices, these devices function at room temperature and do not depend on externally applied magnetic fields. Devices of this type can be designed to function as sensors (exhibiting varying electrical resistance in response to varying temperature, magnetic field, electric field, and/or

mechanical pressure) and as elements of electronic memories.

The underlying principle is that the application of one or more short electrical pulse(s) can induce a reversible, irreversible, or partly reversible change in the electrical, thermal, mechanical, and magnetic properties of a thin perovskite film. The energy in the pulse must be large enough to induce the desired change but not so large as to destroy the film. Depending on the requirements of a specific application, the pulse(s) can

have any of a large variety of waveforms (e.g., square, triangular, or sine) and be of positive, negative, or alternating polarity. In some applications, it could be necessary to use multiple pulses to induce successive incremental physical changes.

In one class of applications, electrical pulses of suitable shapes, sizes, and polarities are applied to vary the detection sensitivities of sensors. Another class of applications arises in electronic circuits in which certain resistance values are required to be variable: Incorporating the

affected resistors into devices of the present type makes it possible to control their resistances electrically over wide ranges, and the lifetimes of electrically variable resistors exceed those of conventional mechanically variable resistors. Another and potentially the most

important class of applications is that of resistance-based nonvolatile-memory devices, such as a resistance random access memory (RRAM) described in the immediately following article, “Electrically Variable Resistive Memory Devices” (MFS-32511-1).

*This work was done by Shangqing Liu, Nai-Juan Wu, and Alex Ignatiev of the University of Houston for Marshall Space Flight Center. For further information, contact Sammy Nabors, MSFC Commercialization Assistance Lead, at sammy.a.nabors@nasa.gov. Refer to MFS-32512-1.*

---

## Two-Dimensional Synthetic-Aperture Radiometer

**Aperture synthesis is employed to reduce antenna mass.**

*Goddard Space Flight Center, Greenbelt, Maryland*

A two-dimensional synthetic-aperture radiometer, now undergoing development, serves as a test bed for demonstrating the potential of aperture synthesis for remote sensing of the Earth, particularly for measuring spatial distributions of soil moisture and ocean-surface salinity. The goal is to use the technology for remote sensing aboard a spacecraft in orbit, but the basic principles of design and operation are applicable to remote sensing from aboard an aircraft, and the prototype of the system under development is designed for operation aboard an aircraft.

In aperture synthesis, one utilizes several small antennas in combination with a signal processing in order to obtain resolution that otherwise would require the use of an antenna with a larger aperture (and, hence, potentially more difficult to deploy in space). The principle upon which this system is based is similar to that of Earth-rotation aperture synthesis employed in radio astronomy. In this technology the coherent products (correlations) of signals from pairs of

antennas are obtained at different antenna-pair spacings (baselines). The correlation for each baseline yields a sample point in a Fourier transform of the brightness-temperature map of the scene. An image of the scene itself is then reconstructed by inverting the sampled transform.

The predecessor of the present two-dimensional synthetic-aperture radiometer is a one-dimensional one, named the Electrically Scanned Thinned Array Radiometer (ESTAR). Operating in the L band, the ESTAR employs aperture synthesis in the cross-track dimension only, while using a conventional antenna for resolution in the along-track dimension.

The two-dimensional instrument also operates in the L band — to be precise, at a frequency of 1.413 GHz in the frequency band restricted for passive use (no transmission) only. The L band was chosen because (1) the L band represents the long-wavelength end of the remote-sensing spectrum, where the problem of achieving adequate spatial resolution is most critical and (2) imag-

ing airborne instruments that operate in this wavelength range and have adequate spatial resolution are difficult to build and will be needed in future experiments to validate approaches for remote sensing of soil moisture and ocean salinity.

The two-dimensional instrument includes a rectangular array of patch antennas arranged in the form of a cross. The ESTAR uses analog correlation for one dimension, whereas the two-dimensional instrument uses digital correlation. In two dimensions, many more correlation pairs are needed and low-power digital correlators suitable for application in spaceborne remote sensing will help enable this technology. The two-dimensional instrument is dual-polarized and, with modification, capable of operating in a polarimetric mode. A flight test of the instrument took place in June 2003 and it participated in soil moisture experiments during the summers of 2003 and 2004.

*This work was done by David M. Le Vine of Goddard Space Flight Center. Further information is contained in a TSP (see page 1). GSC-14809-1*

---

## Ethernet-Enabled Power and Communication Module for Embedded Processors

**This device enables serial-to-Ethernet conversion and provides power to remote locations without adding cables.**

*John F. Kennedy Space Center, Florida*

The power and communications module is a printed circuit board (PCB) that has the capability of providing power to an embedded processor and converting Ethernet packets into serial data to transfer to the processor. The purpose of the new design is to address the shortcomings of previous designs, including

limited bandwidth and program memory, lack of control over packet processing, and lack of support for timing synchronization.

The module includes an RJ-45 with integrated magnetics and power pass-through, integrated Power over Ethernet (PoE) controller, an Ethernet controller

[media access controller (MAC)], a Silicon Laboratories C8051F120 microcontroller with synchronous and asynchronous communication ports, a real-time clock, a hardware watchdog timer, a DC-DC converter with triple output, and 1 Mbit of non-volatile ferroelectric RAM. This new kind of RAM, called FRAM,

does not require a battery backup, yet is has unlimited read and write cycles, and a much smaller access time (60 nanoseconds) than traditional flash memory. The FRAM may be used to store data from the C8051.

The new design of the module creates a robust serial-to-Ethernet conversion that is powered using the existing Ethernet cable. Not only can the module perform these conversions, it also has the processing capability and memory to implement other protocols (like IEEE 1451, IEEE 1588, etc.) and to offload these tasks from other embedded processors.

This innovation has a small form factor that allows it to power processors and transducers with minimal space requirements. The power for the module is provided over the spare pins of the Ethernet CAT-5 cable from Power Source Equipment (PSE) according to IEEE 802.11a.

The power and communication module then converts the power into three different voltage levels: 5 volts DC, +12 volts DC and -12 volts DC, which are provided to the embedded processor or transducer through a power header on the PCB.

The power and communication module is also equipped with an Ethernet Controller and microprocessor that can send and receive Internet Protocol (IP)-based packets over the CAT-5 cable on a 10/100 Megabit Ethernet network. The Ethernet controller takes care of overhead communication with the network, and the microprocessor is able to access packets stored in the Ethernet controller's buffer. The microprocessor translates the packets to and from serial data to packets using a standard serial peripheral interface (SPI). The SPI data can be sent and received to another em-

bedded processor over the digital header on the PCB.

The power and communication module is equipped with a hardware watchdog timer that monitors the SPI communication and resets the processors if communications cease. The power and communication module has the additional feature of a real time clock (RTC) that is used to synchronize the time of the power and communication module and its associated embedded processor(s) with the time of another entity on the Ethernet network. Time synchronization is achieved through a combination of hardware and software using the RTC and IEEE 1588 Precision Time Protocol.

*This work was done by Jose Perotti of Kennedy Space Center, and Carlos Mata and Rebecca Oostdyk of ASRC Aerospace Corp. Further information is contained in a TSP (see page 1). KSC-13112*

---

## Electrically Variable Resistive Memory Devices

**Data are written or read using larger or smaller current pulses, respectively.**

*Marshall Space Flight Center, Alabama*

Nonvolatile electronic memory devices that store data in the form of electrical-resistance values, and memory circuits based on such devices, have been invented. These devices and circuits exploit an electrically-variable-resistance phenomenon that occurs in thin films of certain oxides that exhibit the colossal magnetoresistive (CMR) effect. It is worth emphasizing that, as stated in the immediately preceding article, these devices function at room temperature and do not depend on externally applied magnetic fields.

A device of this type is basically a thin-film resistor: it consists of a thin film of a CMR material located between, and in contact with, two electrical conductors. The application of a short-duration, low-

voltage current pulse via the terminals changes the electrical resistance of the film. The amount of the change in resistance depends on the size of the pulse. The direction of change (increase or decrease of resistance) depends on the polarity of the pulse. Hence, a datum can be written (or a prior datum overwritten) in the memory device by applying a pulse of size and polarity tailored to set the resistance at a value that represents a specific numerical value. To read the datum, one applies a smaller pulse — one that is large enough to enable accurate measurement of resistance, but small enough so as not to change the resistance.

In writing, the resistance can be set to any value within the dynamic range of the CMR film. Typically, the value would

be one of several discrete resistance values that represent logic levels or digits. Because the number of levels can exceed 2, a memory device of this type is not limited to binary data. Like other memory devices, devices of this type can be incorporated into a memory integrated circuit by laying them out on a substrate in rows and columns, along with row and column conductors for electrically addressing them individually or collectively.

*This work was done by Shangqing Liu, Nai-Juan Wu, Alex Ignatiev, and E. J. Charlson of the University of Houston for Marshall Space Flight Center. For more information, contact Sammy Nabors, MSFC Commercialization Assistance Lead, at [sammy.a.nabors@nasa.gov](mailto:sammy.a.nabors@nasa.gov). MFS-32511-1*



## Improved Attachment in a Hybrid Inflatable Pressure Vessel

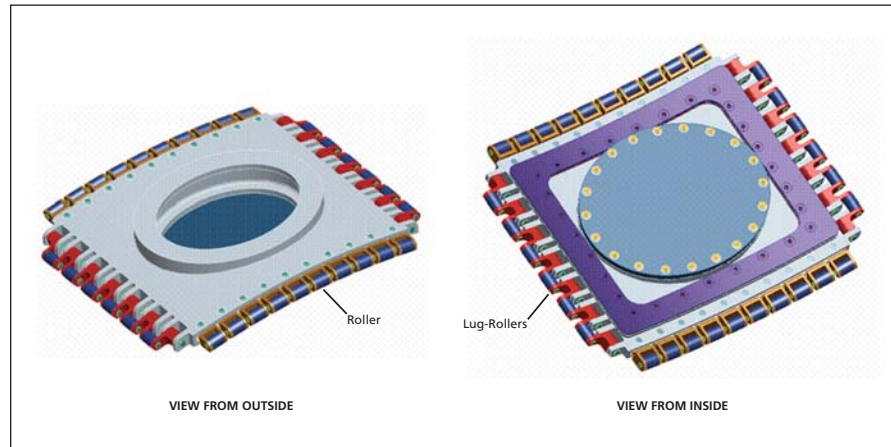
Care is taken to distribute loads and maintain desired shapes.

Lyndon B. Johnson Space Center, Houston, Texas

Some modifications that could be made, separately or together, have been conceived as improvements of the generic design of a structure of the type described in “Hybrid Inflatable Pressure Vessel” (MSC-23024/92), *NASA Tech Briefs*, Vol. 28, No. 4 (April 2004), page 44. To recapitulate: The vessel is a hybrid that comprises an inflatable shell attached to a rigid structure. The inflatable shell is, itself, a hybrid that comprises (1) a pressure bladder restrained against expansion by (2) a restraint layer that comprises a web of straps made from high-strength polymeric fabrics. The present improvements are intended to overcome deficiencies in those aspects of the original design that pertain to attachment of the inflatable shell to the rigid structure. In a typical intended application, such attachment(s) would be made at one or more window or hatch frames to incorporate the windows or hatches as integral parts of the overall vessel.

A detailed description of the deficiencies of the prior design, the modification(s) for overcoming each of them, and alternative versions of the modifications would greatly exceed the space available for this article. The modifications can be summarized as being intended to effect the following improvements with respect to attachment to a window or hatch frame:

- Minimizing the number of straps that pass by the frame unattached and unwoven;
- Sizing the straps to distribute the loads as nearly evenly as possible among the straps in order to minimize both (1) distortion of the inflated shell and the frame from their desired shapes and (2) concentrations of stress that could lead to rupture;
- Ensuring that the restraint layer and bladder conform as closely as possible to the desired restraint-layer shape all the way into the rigid frame, minimizing any effects of discontinuities in shape at the attachments;
- Eliminating gaps between adjacent attachments around the frame to pre-



Rollers and Lug-Rollers that pivot on pin joints in lugs on a frame serve as devices for attachment, to the frame, of straps that restrain an inflated bladder that is sealed to the frame.

vent protrusion of the inflated bladder through the gaps (such protrusion could lead to rupture of the bladder); and

- Preventing entanglement of unwoven straps during inflation of the bladder from the compact, folded condition to the fully deployed condition.

As in the design described in the cited prior article, each end of an attached strap is wrapped around a roller on a pin and stitched to itself at a lap seam. The pin can be supported by a lug on the frame; by a lug-roller that is supported by a pin in a lug on the frame; or by a clevis attached to the frame (see figure). A felt buffer can be placed between the bladder and the restraint layer in the attachment region to serve as a smooth backing for the bladder and to cover any gap through which the bladder could potentially protrude. The felt buffer also helps to ensure the proper relative positioning (thereby helping to prevent entanglement) of any unwoven straps with which it is in contact.

It is very difficult to solve the above-mentioned problem of sizing the straps for several reasons: The straps attached to the frame behave differently from those not attached to the frame, the roller-and-lap-seam portion of each strap attached to the frame is

about twice as stiff as the portion of that strap away from the frame, and the relatively high stiffness of the frame affects the loads on the straps. Different straps become elongated by different amounts and take up different and changing portions of the overall load during the inflation process. If the attached and unattached straps are not sized appropriately with respect to the frame, then the unattached straps, the attached straps, and/or the frame could become excessively elongated or overloaded prematurely (and, consequently, could fail) during the inflation process. Thus, the problem of balancing loads among the straps and frame is complex and highly nonlinear. A computer program was written to solve this problem and was demonstrated by using it to design a restraint-layer/window interface that subsequently passed a pressure test.

*This work was done by Christopher J. Johnson, Ross Patterson, and Gary R. Spexarth of Johnson Space Center. Further information is contained in a TSP (see page 1).*

*This invention is owned by NASA, and a patent application has been filed. Inquiries concerning nonexclusive or exclusive license for its commercial development should be addressed to the Patent Counsel, Johnson Space Center, (281) 483-0837. Refer to MSC-24201-1/73-1.*

---

## Electrostatic Separator for Beneficiation of Lunar Soil

Process complexity may be significantly reduced.

*John F. Kennedy Space Center, Florida*

A charge separator has been constructed for use in a lunar environment that will allow for separation of minerals from lunar soil. Any future lunar base and habitat must be constructed from strong, dense materials to provide for thermal and radiation protection. It has been proposed that lunar soil may meet this need, and sintering of full-scale bricks has been accomplished using lunar simulant. In the present experiments, whole lunar dust as received was used. The approach taken here was that beneficiation of ores into an industrial feedstock grade may be more efficient. Refinement or enrichment of specific minerals in the soil before it is chemically processed may be more desirable as it would reduce the size and energy requirements necessary to produce the virgin material, and it may significantly reduce the process complexity.

The principle is that minerals of different composition and work function will charge differently when tribocharged against different materials, and hence be separated in an electric

field. The charge separator is constructed of two parallel copper plates separated by a variable distance in a vacuum-compatible box. The top and bottom of the box are designed so that the separation and angle between the plates can be varied. The box has a removable front plate for access, and each plate is connected to a high-voltage, vacuum-compatible connector that connects to feedthroughs in a vacuum chamber. Each plate is respectively powered by positive and negative high-voltage regulated DC power modules. Tribocharged dust is fed into the top through a small hole, where it is subjected to an intense electric field generated between the plates. Positively charged particles will be attracted to the negative plate, while negatively charged particles will be attracted to the positive plate. Dust collected on each plate and on filter paper in the collection box at the bottom of the plates can then be weighed to determine the mass-fraction separation.

Because this device is meant for use in a lunar environment, much higher

voltages can be used where there is no gas breakdown. Special care was taken in the design of the high-voltage connections to the separator plates. Pure copper plates and other materials were chosen for their low outgassing properties. Modeling of particle trajectories within the plates showed that for the Q/M (charge to mass ratio) measurements of the charged particles in vacuum, a smaller, more compact separator can be used on the Moon compared to the same device on Earth. Another advantage of this design is that, in the lower gravity environment of the Moon, particles will spend more time falling between the plates. Again, a smaller device and higher voltages can use this advantage to increase the efficiency of the lunar soil beneficiation process.

*This work was done by Jacqueline Quinn, and Ellen Arens of NASA Kennedy Space Center, Steve Trigwell of ASRC Aerospace, and James Captain of the University of Central Florida. Further information is contained in a TSP (see page 1). KSC-13007*





## Amorphous Rover

This rover would maneuver on terrain by altering its shape.

*Goddard Space Flight Center, Greenbelt, Maryland*

A proposed mobile robot, denoted the amorphous rover, would vary its own size and shape in order to traverse terrain by means of rolling and/or slithering action. The amorphous rover was conceived as a robust, lightweight alternative to the wheeled rover-class robotic vehicle heretofore used in exploration of Mars. Unlike a wheeled rover, the amorphous rover would not have a pre-

defined front, back, top, bottom, or sides. Hence, maneuvering of the amorphous rover would be more robust: the amorphous rover would not be vulnerable to overturning, could move backward or sideways as well as forward, and could even narrow itself to squeeze through small openings. Examples of potential terrestrial applications of the amorphous rover include exploration or

military reconnaissance on rough terrain, inspection inside narrow tunnels, and searching for victims trapped in rubble of collapsed buildings.

The main structure of the amorphous rover would consist of a tetrahedral mesh of nodes connected by variable-length struts, covered with a stretchable fabric connected to the outer nodes (see Figure 1). The rolling and/or slithering

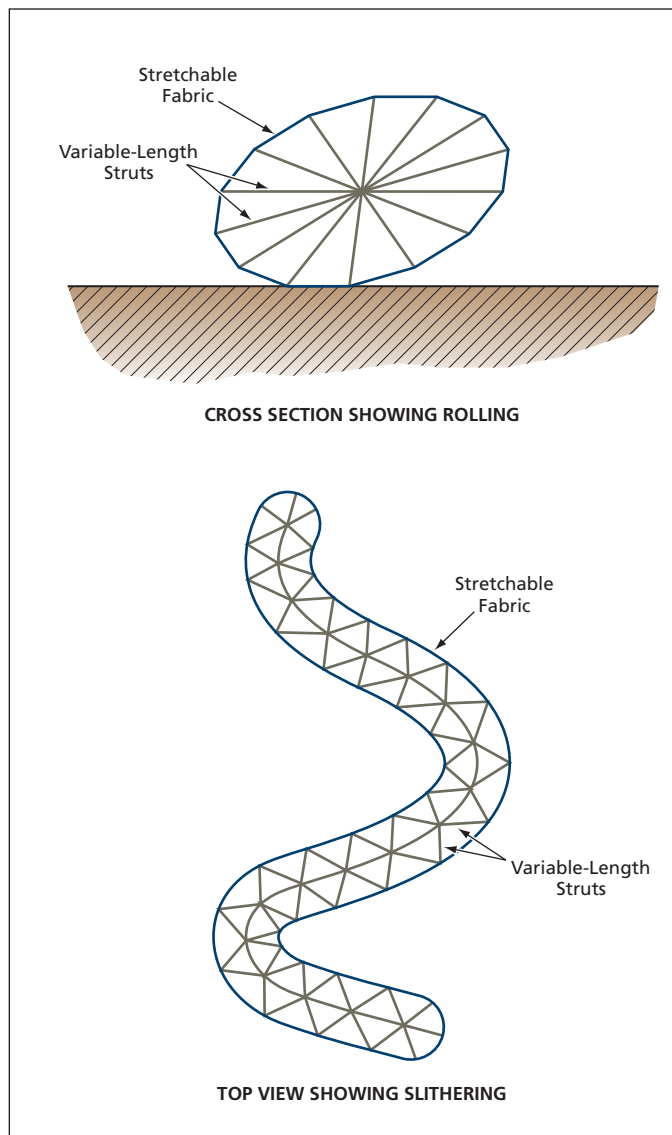


Figure 1. A Tetrahedral Mesh of Variable-Length Struts would be enclosed by a stretchable fabric. Struts would be lengthened and/or shortened in coordination to effect rolling and/or slithering.

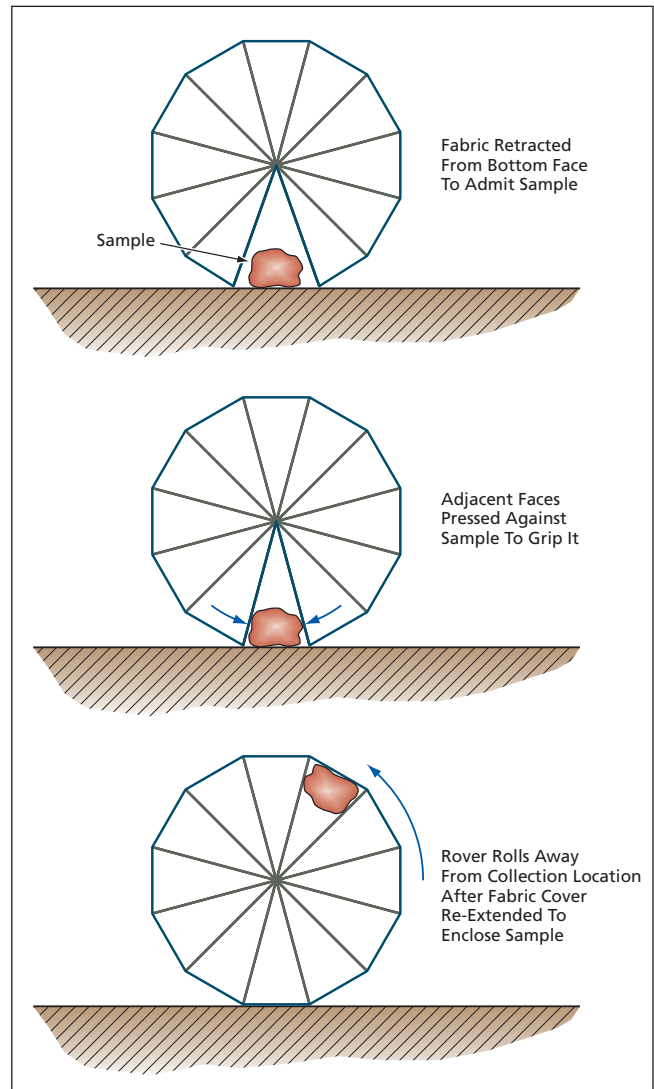


Figure 2. A Sample Would Be Collected by momentarily retracting the fabric from one of the outer faces, rotating so that a tetrahedral compartment that includes the open face contains the sample, re-extending the fabric to cover the outer face and trap the sample inside, then rolling away from the collection position.

action would be effected through coordinated lengthening and shorting of the struts. Inasmuch as there would be no head, visual and/or other data needed for navigation would be obtained by means of a distributed sensor network inside the structure. A sample for return could be collected by a process, illustrated in Figure 2, that would lead to retention of the sample in a tetrahedral

compartment defined by stretchable fabric covering all its faces.

The amorphous rover could, in principle, be designed and built using currently available macroscopic electromechanical components. In addition, the basic amorphous-rover concept admits of a numerous design variations, including ones involving extreme miniaturization through exploitation of microelectromechanical systems

(MEMS), nanoelectromechanical systems (NEMS), and perhaps even the use of carbon nanotubes. Any or all of these variations could include control systems based on evolvable neural software systems.

*This work was done by Steven A. Curtis of Goddard Space Flight Center. For further information, contact the Goddard Innovative Partnerships Office at (301) 286-5810. GSC-14850-1*

## ⚙️ Space-Frame Antenna

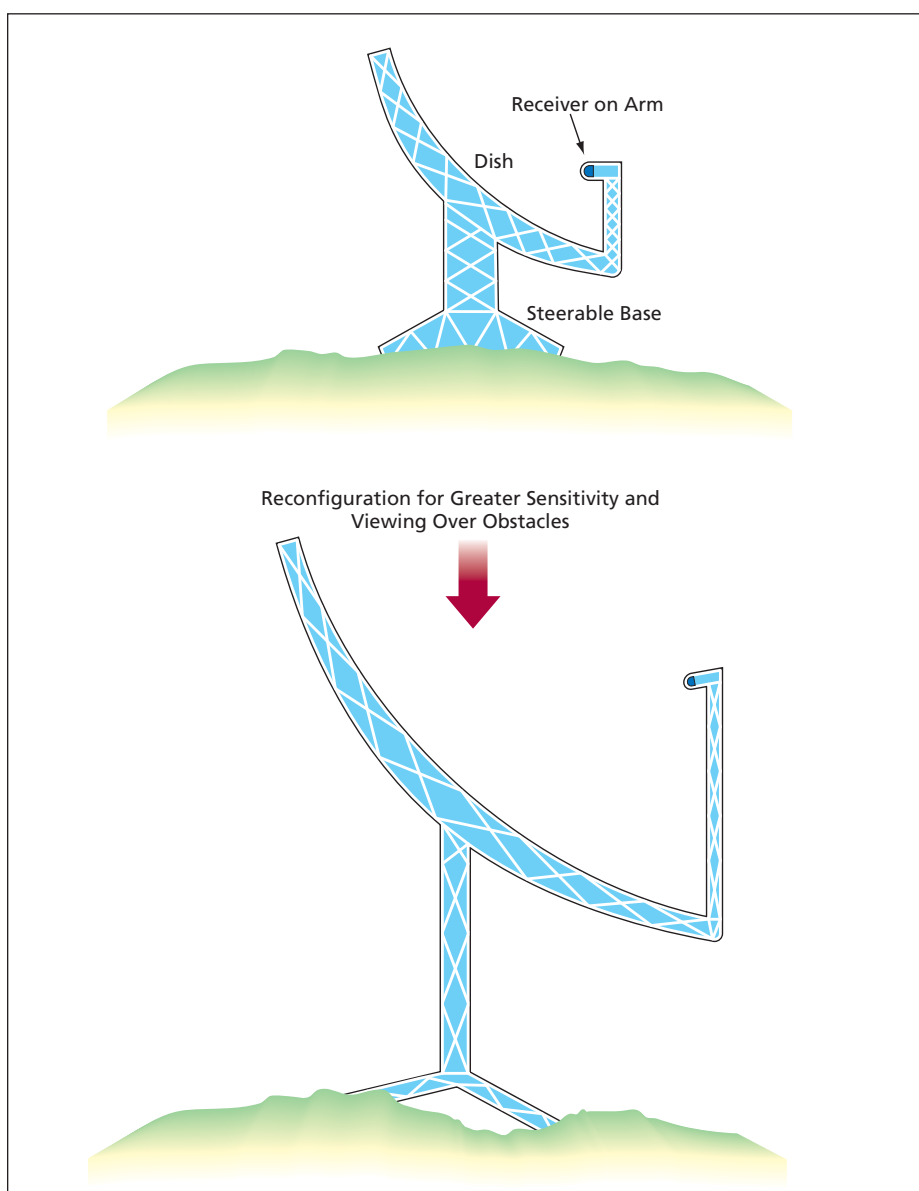
**The structure could be deformed to a desired size, shape, and orientation.**

*Goddard Space Flight Center, Greenbelt, Maryland*

The space-frame antenna is a conceptual antenna structure that would be lightweight, deployable from compact stowage, and capable of deforming itself to a size, shape, and orientation required for a specific use. The underlying mechanical principle is the same as that of the amorphous rover described in the immediately preceding article: The space-frame antenna would be a trusslike structure consisting mostly of a tetrahedral mesh of nodes connected by variable-length struts. (The name of the antenna reflects the fact that such a structure has been called a “space frame.”) The deformation of the antenna to a desired size, shape, and orientation would be effected through coordinated lengthening and shorting of the struts. In principle, it would even be possible to form the space-frame antenna by deforming another space-frame structure (e.g., the amorphous rover) in this manner.

Typically, the space-frame antenna would be configured as a dish-type reflector with an arm holding a receiver, all on a steerable base. Examples of exploiting the space-frame concept to reconfigure the antenna for a specific use include making the base taller (for viewing over obstructions) and making the dish wider (for greater sensitivity), as illustrated in the figure.

Like the amorphous rover, the space-frame antenna could be designed and built using currently available macroscopic electromechanical components or by exploiting microelectromechanical systems (MEMS), nanoelectromechanical systems (NEMS), or perhaps even carbon



The Antenna Could Be Widened and Heightened as shown here for better viewing and greater sensitivity. It could also be twisted, reoriented, and/or otherwise deformed to aim it in one or more different direction(s).

nanotubes. An initial version made from currently available components would likely have an areal mass density of the order of 1 kg/m<sup>2</sup>. More-advanced versions made from MEMS, NEMS, or nanotubes could have areal mass densi-

ties ranging from about 100 to as little as 10 g/m<sup>2</sup>. Also as in the case of the amorphous rover, any or all of these versions could include control systems based partly on evolvable neural software systems.

*This work was done by Steven A. Curtis of Goddard Space Flight Center. For further information, contact the Goddard Innovative Partnerships Office at (301) 286-5810. GSC-14849-1*

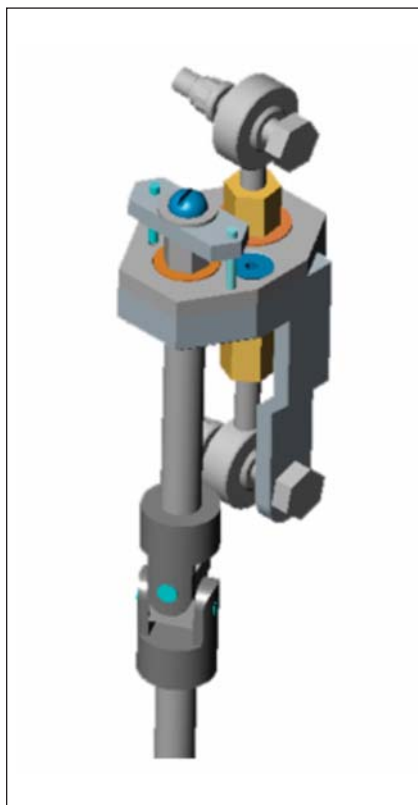
## ⚙️ Gear-Driven Turnbuckle Actuator

**This tool allows for continued adjustments to turnbuckles without the need to remove them.**

*John H. Glenn Research Center, Cleveland, Ohio*

This actuator design allows the extension and contraction of turnbuckle assemblies. It can be operated manually or remotely, and is extremely compact. It is ideal for turnbuckles that are hard to reach by conventional tools. The tool assembly design solves the problem of making accurate adjustments to the variable geometry guide vanes without having to remove and reinstall the actuator system back on the engine. The actuator does this easily by adjusting the length of the turnbuckles while they are still attached to the engine.

Made out of metal, the actuator has three components: a gear case, a locking mechanism, and a driver bar. It operates by attaching the gear case around the turnbuckle, then securing the gears with the locking mechanism, and finally making adjustments by turning the driver bar. The gear case consists of two gears and a stabilizing arm. The first gear, the ratcheting gear, is used to make adjustments. The second gear, the turnbuckle gear, operates the turnbuckle, and the stabilizing arm secures the gear case in place. The gear rivet nut of the driver bar fits into the adjustment gear. Manually turning the driver bar rotates the adjustment gear, which in turn engages the turnbuckle gear. As the turnbuckle gear rotates, adjustments are made to the turnbuckle. The stabilizing arm prevents the turn-



The **Tool Assembly** adjusts the length of the turnbuckle while it is still attached to the engine, eliminating the problem of removing and installing the actuator system back onto the engine.

buckle case from rotating when the driver arm is operated, and the arm is securely attached to the turnbuckle assembly.

To prevent gear movement due to vibration, a locking mechanism secures the gears once adjustments are made. Tool operation is straightforward — the driver bar is turned either clockwise or counterclockwise to lengthen or shorten the turnbuckle. The angle of the guide vanes is read out using encoders mounted on the engine. When the desired offset angle is reached, the locking mechanism is engaged, thus securing the length of the turnbuckle. What would originally have taken a day to accomplish is now done in approximately ten minutes, and with greater accuracy, because the turnbuckle is never removed. The effectiveness of this tool is best appreciated when one considers a typical engine, with four or more turnbuckles, where each turnbuckle requires several configurations to make vane readings.

*This work was done by Ricky N. Rivera of Glenn Research Center. Further information is contained in a TSP (see page 1).*

*Inquiries concerning rights for the commercial use of this invention should be addressed to NASA Glenn Research Center, Innovative Partnerships Office, Attn: Steve Fedor, Mail Stop 4-8, 21000 Brookpark Road, Cleveland, Ohio 44135. Refer to LEW-18427-1.*

## ⚙️ In-Situ Focusing Inside a Thermal Vacuum Chamber

**This method would enable less expensive, faster focusing for IR imaging cameras and spectrometers.**

*NASA's Jet Propulsion Laboratory, Pasadena, California*

Traditionally, infrared (IR) space instruments have been focused by iterating with a number of different thickness shim rings in a thermal vacuum chamber until the focus meets requirements. This has required a number of thermal

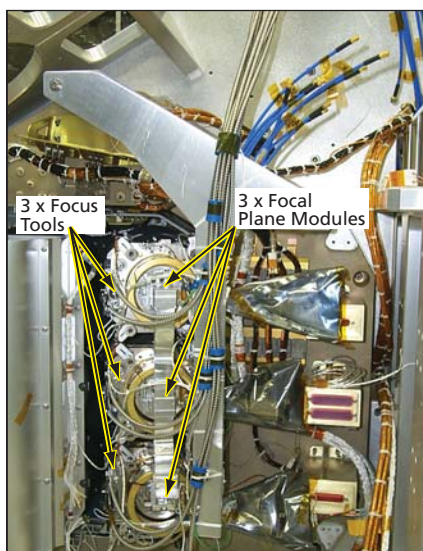
cycles that are very expensive as they tie up many integration and test (I&T)/environmental technicians/engineers working three shifts for weeks. Rather than creating a test shim for each iteration, this innovation replaces the test

shim and can focus the instrument while in the thermal vacuum chamber.

The focus tool consists of three small, piezo-actuated motors that drive two sets of mechanical interface flanges between the instrument optics and the focal-plane

assembly, and three optical-displacement metrology sensors that can be read from outside the thermal vacuum chamber. The motors are used to drive the focal planes to different focal distances and acquire images, from which it is possible to determine the best focus. At the best focus position, the three optical displacement metrology sensors are used to determine the shim thickness needed. After the instrument leaves the thermal vacuum chamber, the focus tool is replaced with the precision-ground shim ring.

The focus tool consists of two sets of collars, one that mounts to the backside of the interface flange of the instrument optics, and one that mounts to the backside of the interface flange of the focal plane modules. The collars on the instrument optics side have the three small piezo-actuated motors and the three optical displacement metrology systems. Before the instrument is focused, there is no



The three **Focal-Plane Modules** and the **Focus Tools** are shown on the OCO flight instrument, where space was very tight. The image was taken before thermal blanketing was installed.

shim ring in place and, therefore, no fasteners holding the focal plane modules to the cameras. Two focus tooling collars are held together by three strong springs.

The Orbiting Carbon Observatory (OCO) mission spectrometer was focused this way (see figure). The motor described here had to be moved five times to reach an acceptable focus, all during the same thermal cycle, which was verified using pupil slicing techniques. A focus accuracy of  $\approx 20$ – $100$  microns was achieved.

*This work was done by Carl Christian Liebe, Brett Hannah, Randall Bartman, Costin Radulescu, Mayer Rud, Edwin Sarkissian, and Timothy Ho of Caltech; Randy Pollock, Joseph Esposito, Brian Sutin, and Robert Haring of Hamilton Sundstrand Corp.; and Juan Gonzalez (contractor) for NASA's Jet Propulsion Laboratory. For further information, contact [iaoffice@jpl.nasa.gov](mailto:iaoffice@jpl.nasa.gov). NPO-45749*

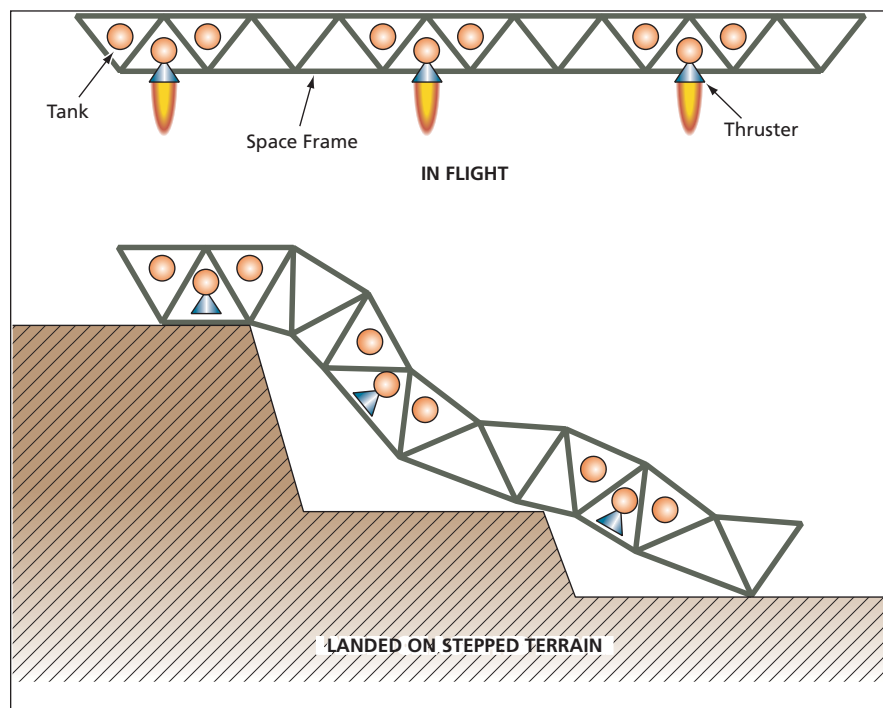
## ⚙️ Space-Frame Lunar Lander

**This structure would deform itself to sit stably on rough terrain.**

*Goddard Space Flight Center, Greenbelt, Maryland*

The space-frame lunar lander is a conceptual spacecraft or spacecraftlike system based largely on the same principles as those of the amorphous rover and the space-frame antenna described in the two immediately preceding articles. The space-frame lunar lander was originally intended to (1) land on rough lunar terrain, (2) deform itself to conform to the terrain so as to be able to remain there in a stable position and orientation, and (3) if required, further deform itself to perform various functions. In principle, the space-frame lunar lander could be used in the same way on Earth, as might be required, for example, to place meteorological sensors or a radio-communication relay station on an otherwise inaccessible mountain peak.

Like the amorphous rover and the space-frame antenna, the space-frame lunar lander would include a trusslike structure consisting mostly of a tetrahedral mesh of nodes connected by variable-length struts, the lengths of which would be altered in coordination to impart the desired overall size and shape to the structure. Thrusters (that is, small rocket engines), propellant tanks, a control system, and instrumentation would be mounted in and on the struc-



A **Spacecraftlike System** looking like a truss equipped with thrusters would land on and conform to an irregular terrain surface.

ture (see figure). Once it had landed and deformed itself to the terrain through coordinated variations in the lengths of the struts, the structure

could be further deformed into another space-frame structure (e.g., the amorphous rover or the space-frame antenna).

Also like the amorphous rover and the space-frame antenna, the space-frame lunar lander could be designed and built using currently available macroscopic electromechanical components or by exploiting microelectromechanical systems (MEMS), nano-

electromechanical systems (NEMS), or carbon nanotubes, and any or all of these versions could include control systems based partly on evolvable neural software systems. The areal mass densities of these versions are expected to be comparable to those of

the corresponding versions of the space-frame antenna.

*This work was done by Steven A. Curtis of Goddard Space Flight Center. For further information, contact the Goddard Innovative Partnerships Office at (301) 286-5810. GSC-14848-1*





## Wider-Opening Dewar Flasks for Cryogenic Storage

Lyndon B. Johnson Space Center, Houston, Texas

Dewar flasks have been proposed as containers for relatively long-term (25 days) storage of perishable scientific samples or other perishable objects at a temperature of  $-175\text{ }^{\circ}\text{C}$ . The refrigeration would be maintained through slow boiling of liquid nitrogen ( $\text{LN}_2$ ). For the purposes of the application for which these containers were proposed, (1) the neck openings of commercial off-the-shelf (COTS) Dewar flasks are too small for most NASA samples; (2) the round shapes of the COTS containers give rise to unacceptably low efficiency of packing in rec-

tangular cargo compartments; and (3) the COTS containers include metal structures that are too thermally conductive, such that they cannot, without exceeding size and weight limits, hold enough  $\text{LN}_2$  for the required long-term-storage.

In comparison with COTS Dewar flasks, the proposed containers would be rectangular, yet would satisfy the long-term storage requirement without exceeding size and weight limits; would have larger neck openings; and would have greater sample volumes, leading to a packing efficiency of about double the sample volume as a

fraction of total volume. The proposed containers would be made partly of aerospace-type composite materials and would include vacuum walls, multilayer insulation, and aerogel insulation.

*This work was done by Warren P. Ruemele of Johnson Space Center; John Manry, Kristin Stafford, and Grant Bue of Lockheed Martin Corp.; George R. Rowland, Jr., and John Krejci of Hernandez Engineering; and Bent Evernden of Rothe Joint Venture, L.P. For further information, contact the Johnson Commercial Technology Office at (281) 483-3809. MSC-23761-1*

## Silicon Oxycarbide Aerogels for High-Temperature Thermal Insulation

Marshall Space Flight Center, Alabama

This work has shown that the use of SOC-A35 leads to aerogel materials containing a significant concentration of carbidic species and limited amorphous free carbon. Substitution of the divalent oxide species in silica with trivalent carbidic carbon has directly led to materials that exhibit increased

network viscosity, reduced sintering, and limited densification. The SiOC aerogels produced in this work have the highest carbide content of any dense or porous SiOC glass reported in the literature at that time, and exhibit tremendous long-term thermal stability.

*This work was done by Owen Evans, Wendell Rhine, and Decio Coutinho of Aspen Aerogels, Inc. for Marshall Space Flight Center. For further information, contact Sammy Nabors, MSFC Commercialization Assistance Lead, at [sammy.a.nabors@nasa.gov](mailto:sammy.a.nabors@nasa.gov). Refer to MFS-32692-1.*

## Supercapacitor Electrolyte Solvents With Liquid Range Below $-80\text{ }^{\circ}\text{C}$

New formulations extend operation into lower temperatures.

NASA's Jet Propulsion Laboratory, Pasadena, California

A previous NASA Tech Brief ["Low-Temperature Supercapacitors" (NPO-44386) *NASA Tech Briefs*, Vol. 32, No 7 (July 2008), page 32] detailed ongoing efforts to develop non-aqueous supercapacitor electrolytes capable of supporting operation at temperatures below commercially available cells (which are typically limited to charging and discharging at  $\geq -40\text{ }^{\circ}\text{C}$ ). These electrolyte systems may enable energy storage and power delivery for systems operating in extreme environments, such as those encountered in the Polar

regions on Earth or in the exploration of space. Supercapacitors using these electrolytes may also offer improved power delivery performance at moderately low temperatures (e.g.,  $-40$  to  $0\text{ }^{\circ}\text{C}$ ) relative to currently available cells, offering improved cold-cranking and cold-weather acceleration capabilities for electrical or hybrid vehicles.

Supercapacitors store charge at the electrochemical double-layer, formed at the interface between a high surface area electrode material and a liquid electrolyte. The current approach to extend-

ing the low-temperature limit of the electrolyte focuses on using binary solvent systems comprising a high-dielectric-constant component (such as acetonitrile) in conjunction with a low-melting-point co-solvent (such as organic formates, esters, and ethers) to depress the freezing point of the system, while maintaining sufficient solubility of the salt.

Recent efforts in this area have led to the identification of an electrolyte solvent formulation with a freezing point of  $-85.7\text{ }^{\circ}\text{C}$ , which is achieved by using a 1:1 by volume ratio of acetonitrile to 1,3-dioxolane

(as determined by differential scanning calorimetry). This is in contrast to a freezing point of  $-45.7\text{ }^{\circ}\text{C}$  for the pure acetonitrile solvent used in typical supercapacitor cells. This solvent system readily solubilizes salts commonly used in supercapacitor electrolytes, such as tetraethylammonium tetrafluoroborate (TEATFB) and lithium hexafluorophosphate.

Full electrolyte systems were formulated through the addition of TEATFB to the 1:1 solvent blend, over a range of salt concentrations. Coin cells were then filled with the var-

ious electrolytes for low-temperature electrical testing. Commercially available high surface area carbon-based materials were used as the electrode material, in conjunction with a polyethylene-based separator material. Representative DC discharge data for the 0.50 M concentration system have shown a highly linear discharge over a wide range of temperatures (with little fade in capacitance at the lowest measured temperatures).

*This work was done by Erik Brandon, Marshall Smart, and William West of Caltech for NASA's Jet Propulsion Laboratory.*

*In accordance with Public Law 96-517, the contractor has elected to retain title to this invention. Inquiries concerning rights for its commercial use should be addressed to:*

*Innovative Technology Assets Management  
JPL*

*Mail Stop 202-233*

*4800 Oak Grove Drive*

*Pasadena, CA 91109-8099*

*E-mail: iaoffice@jpl.nasa.gov*

*Refer to NPO-44855, volume and number of this NASA Tech Briefs issue, and the page number.*

## Designs and Materials for Better Coronagraph Occulting Masks

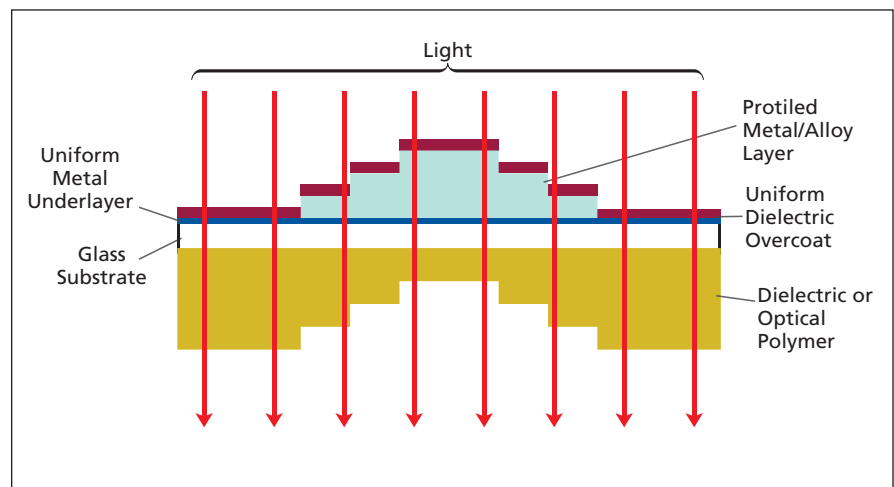
Optical density and phase profiles are achromatized over a broad wavelength range.

NASA's Jet Propulsion Laboratory, Pasadena, California

New designs, and materials appropriate for such designs, are under investigation in an effort to develop coronagraph occulting masks having broad-band spectral characteristics superior to those currently employed. These designs and materials are applicable to all coronagraphs, both ground-based and spaceborne. This effort also offers potential benefits for the development of other optical masks and filters that are required (1) for precisely tailored spatial transmission profiles, (2) to be characterized by optical-density neutrality and phase neutrality (that is, to be characterized by constant optical density and constant phase over broad wavelength ranges), and/or (3) not to exhibit optical-density-dependent phase shifts.

The need for this effort arises for the following reasons:

- Coronagraph occulting masks are required to impose, on beams of light transmitted through them, extremely precise control of amplitude and phase according to carefully designed transmission profiles.
- In the original application that gave rise to this effort, the concern has been to develop broad-band occulting masks for NASA's Terrestrial Planet Finder coronagraph. Until now, experimental samples of these masks have been made from high-energy-beam-sensitive (HEBS) glass, which becomes locally dark where irradiated with a high-energy electron beam, the amount of darkening depending on the electron-beam energy and dose. Precise mask profiles have been written on HEBS glass blanks by use of electron beams,



**Thin Metal and Dielectric Films** would be deposited on a glass substrate. Their thicknesses would be stepped to obtain a specified spatial transmission profile with a uniform phase profile. This drawing is simplified and is not to scale.

and the masks have performed satisfactorily in monochromatic light. However, the optical-density and phase profiles of the HEBS masks vary significantly with wavelength; consequently, the HEBS masks perform unsatisfactorily in broad-band light.

The key properties of materials to be used in coronagraph occulting masks are their extinction coefficients, their indices of refraction, and the variations of these parameters with wavelength. The effort thus far has included theoretical predictions of performances of masks that would be made from alternative materials chosen because the wavelength dependences of their extinction coefficients and their indices of refraction are such that the optical-density and phase profiles of masks made from these materials can be expected to

vary much less with wavelength than do those of masks made from HEBS glass. The alternative materials considered thus far include some elemental metals such as Pt and Ni, metal alloys such as Inconel, metal nitrides such as TiN, and dielectrics such as  $\text{SiO}_2$ .

A mask as now envisioned would include thin metal and dielectric films having stepped or smoothly varying thicknesses (see figure). The thicknesses would be chosen, taking account of the indices of refraction and extinction coefficients, to obtain an acceptably close approximation of the desired spatial transmittance profile with a flat phase profile.

*This work was done by Kunjithapatham Balasubramanian of Caltech for NASA's Jet Propulsion Laboratory. For more information, contact iaoffice@jpl.nasa.gov. NPO-44461*



## Fuel-Cell-Powered Vehicle With Hybrid Power Management

Fuel cells and hydride fuel storage are combined with ultracapacitor energy storage.

John H. Glenn Research Center, Cleveland, Ohio

Figure 1 depicts a hybrid electric utility vehicle that is powered by hydrogen-burning proton-exchange-membrane (PEM) fuel cells operating in conjunction with a metal hydride hydrogen-storage unit. Unlike conventional hybrid electric vehicles, this vehicle utilizes ultracapacitors, rather than batteries, for storing electric energy.

This vehicle is a product of continuing efforts to develop the technological discipline known as hybrid power management (HPM), which is oriented toward integration of diverse electric energy-generating, energy-storing, and energy-consuming devices in optimal configurations. Instances of HPM were reported in five prior *NASA Tech Briefs* articles, though not explicitly labeled as HPM in the first three articles: “Ultracapacitors Store Energy in a Hybrid Electric Vehicle” (LEW-16876), Vol. 24, No. 4 (April 2000), page 63; “Photovoltaic Power Station With Ultracapacitors for Storage” (LEW-17177), Vol. 27, No. 8 (August 2003), page 38; “Flasher Powered by Photovoltaic Cells and Ultracapacitors” (LEW-17246), Vol. 27, No. 10 (October 2003), page 37; “Hybrid Power Management” (LEW-17520), Vol. 29, No. 12 (December 2005), page 35; and “Ultracapacitor-Powered Cordless Drill” (LEW-18116-1), Vol. 31, No. 8 (August 2007), page 34.

To recapitulate from the cited prior articles: The use of ultracapacitors as energy-storage devices lies at the heart of HPM. An ultracapacitor is an electrochemical energy-storage device, but unlike in a conventional rechargeable electrochemical cell or battery, chemical reactions do not take place during operation. Instead, energy is stored electrostatically at an electrode/electrolyte interface. The capacitance per unit volume of an ultracapacitor is much greater than that of a conventional capacitor because its electrodes have much greater surface area per unit volume and the separation between the electrodes is much smaller.

In comparison with conventional power management in which batteries are used to store energy, HPM offers many advantages, including the following:



Figure 1. This Fuel-Cell-Powered Utility Vehicle has been used to demonstrate the practicability of hybrid power management.

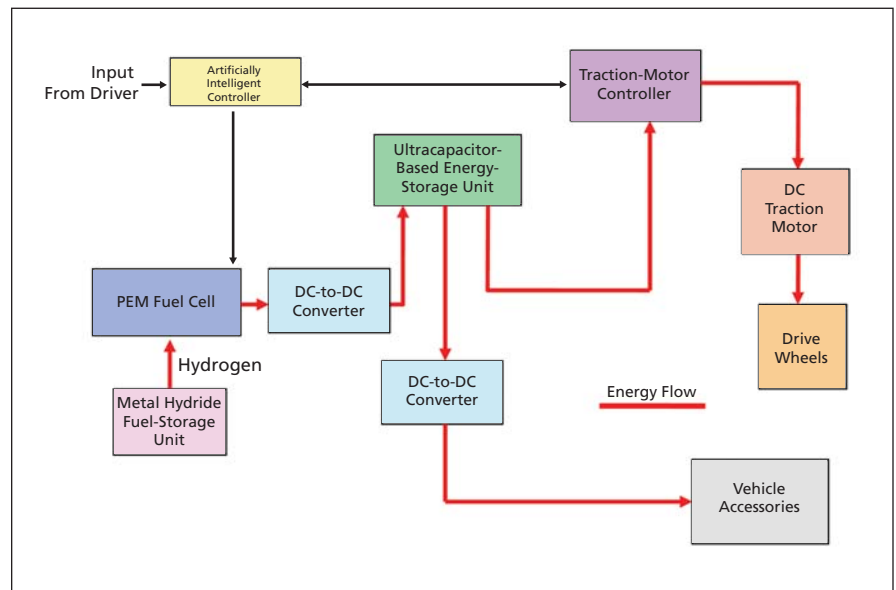


Figure 2. The HPM System of the vehicle shown in Figure 1 differs from the power-management systems of conventional hybrid electric vehicles in several major features, including the use of fuel cells (instead of an internal-combustion engine), the use of hydrogen as the fuel, the storage of hydrogen in the form of a metal hydride (instead of a compressed or liquefied gas), and the use of ultracapacitors (instead of batteries) for storing electric energy.

- Power-control circuits for ultracapacitors can be simpler than those for batteries.
- Whereas a typical battery can be charged and discharged about 300 times, an ultracapacitor can be charged and discharged more than a million times.
- The longer lifetimes of ultracapacitors greatly reduce life-of-system costs and reduce adverse environmental effects, inasmuch as it will probably never be necessary to replace and dispose of ultracapacitors in most applications, whereas batteries must be replaced frequently.
- Disposal problems and the associated contributions to life-of-system costs are further reduced because the chemical constituents of ultracapacitors are less toxic and less environmentally harmful than are those of batteries.
- Excellent low-temperature performance makes ultracapacitors suitable for storing energy in applications at temperatures too low for batteries.
- The consistent performance of ultracapacitors over time enables reliable operation not possible with batteries.
- Unlike batteries, ultracapacitors can be safely left completely discharged for indefinitely long times.

- Whereas the charge-discharge efficiency in conventional power management using rechargeable batteries is typically about 50 percent, the charge-discharge efficiency in HPM typically exceeds 90 percent.

Figure 2 depicts the relationships among the various subsystems of the HPM system for the present fuel-cell-powered utility vehicle. At the beginning of operation, the PEM fuel cells are started and used to charge the ultracapacitors. As operation continues, the fuel cells continue to recharge the ultracapacitors while electric energy is drawn from the ultracapacitors (just as energy is drawn from a rechargeable battery in a conventional hybrid vehicle) to drive an electric traction motor that propels the vehicle. In a conceptual alternative version of the vehicle, photovoltaic cells would be used (in addition to or instead of fuel cells) to charge the ultracapacitors. In another conceptual version, some additional recharging would be gained by use of regenerative braking.

Large transient loads are imposed on the traction motor of this or any electric vehicle. Large transient loads shorten the operational lifetimes of PEM fuel cells. By smoothing out the

transient loads applied to the PEM fuel cells, the energy-storage devices (in this case, the ultracapacitors) increase the operational lifetimes of the fuel cells and make it possible to utilize fuel cells smaller than would be necessary if the fuel cells alone were required to satisfy the peak power demand. An optimized combination of PEM fuel cells and ultracapacitors makes it possible to obtain high energy and power densities.

The storage of the hydrogen fuel in the form of a metal hydride is a major feature of the design of this system, intended to overcome the disadvantages of the prior approaches to storing hydrogen as a compressed gas at room temperature or as a cryogenic liquid. Storage in a metal hydride can be accomplished more safely and efficiently, at relatively low pressure, without refrigeration.

*This work was done by Dennis J. Eichenberg of Glenn Research Center. Further information is contained in a TSP (see page 1).*

*Inquiries concerning rights for the commercial use of this invention should be addressed to NASA Glenn Research Center, Innovative Partnerships Office, Attn: Steve Fedor, Mail Stop 4-8, 21000 Brookpark Road, Cleveland, Ohio 44135. Refer to LEW-18281-1.*

## Fine-Water-Mist Multiple-Orientation-Discharge Fire Extinguisher

Rechargeable system discharges 100 percent of its contents regardless of extinguisher orientation.

*John H. Glenn Research Center, Cleveland, Ohio*

A fine-water-mist fire-suppression device has been designed so that it can be discharged uniformly in any orientation via a high-pressure gas propellant. Standard fire extinguishers used while slightly tilted or on their side will not discharge all of their contents. Thanks to the new design, this extinguisher can be used in multiple environments such as aboard low-gravity spacecraft, airplanes, and aboard vehicles that may become overturned prior to or during a fire emergency. Research in recent years has shown that fine water mist can be an effective alternative to Halons now banned from manufacture.

Currently, NASA uses carbon dioxide for fire suppression on the International Space Station (ISS) and Halon chemical extinguishers on the space shuttle. While each of these agents is effective, they have drawbacks. The toxicity of carbon dioxide requires that the

crew don breathing apparatus when the extinguishers are deployed on the ISS, and Halon use in future spacecraft has been eliminated because of international protocols on substances that destroy atmospheric ozone. A major advantage to the new system on occupied spacecraft is that the discharged system is locally rechargeable. Since the only fluids used are water and nitrogen, the system can be recharged from stores of both carried aboard the ISS or spacecraft. The only support requirement would be a pump to fill the water and a compressor to pressurize the nitrogen propellant gas. This system uses a gaseous agent to pressurize the storage container as well as to assist in the generation of the fine water mist.

The portable fire extinguisher hardware works like a standard fire extinguisher with a single storage container for the agents (water and nitrogen), a

control valve assembly for manual actuation, and a discharge nozzle. The design implemented in the proof-of-concept experiment successfully extinguished both open fires and fires in baffled enclosures.

The proof-of-concept design weighs less than 20 lb (9 kg) and can be easily scaled up or down in size depending on the application. The design is fully self-contained and modular with no complex piping to thread through a crowded habitation module, and mounting is simplified.

The liquid agent is water, or water with additives to enhance the fire suppression capability for specific fire hazards. Compatible gases include nitrogen, argon, or other common nonflammable gases. Each fluid constituent is held in the container by a valve. Design features inside the storage tank make it possible to easily discharge all of the fluid as a uniformly dispersed

fine water mist regardless of gravity or system orientation.

When the system is operated, the gas pressure forces the liquid from the extinguisher. The gas and liquid constituents are also mixed to deliver a multiphase flow to the discharge nozzle to

generate fine water-mist droplets, which extinguish the fire.

*This work was done by James R. Butz, Craig S. Turchi, and Amanda Kimball of ADA Technologies Inc. and Thomas McKinnon and Edward Riedel of Colorado School of Mines for Glenn Research Center.*

*Inquiries concerning rights for the commercial use of this invention should be addressed to ADA Technologies Inc, Attn: Nick Knowlton, 8100 Shaffer Pkwy, suite 130, Littleton, CO. 80127-4107, (303) 874-7377. LEW-18190-1*

---

## Fuel-Cell Water Separator

**Separator uses no moving parts or other power-consuming components.**

*John H. Glenn Research Center, Ohio*

The main product of a typical fuel cell is water, and many fuel-cell configurations use the flow of excess gases (i.e., gases not consumed by the reaction) to drive the resultant water out of the cell. This two-phase mixture then exits through an exhaust port where the two fluids must again be separated to prevent the fuel cell from flooding and to facilitate the reutilization of both fluids.

The Glenn Research Center (GRC) has designed, built, and tested an innovative fuel-cell water separator that not only removes liquid water from a fuel cell's exhaust ports, but does so with no moving parts or other power-consuming components. Instead it employs the potential and kinetic energies already present in the moving exhaust flow. In addition, the

geometry of the separator is explicitly intended to be integrated into a fuel-cell stack, providing a direct mate with the fuel cell's existing flow ports. The separator is also fully scalable, allowing it to accommodate a wide range of water removal requirements. Multiple separators can simply be "stacked" in series or parallel to adapt to the water production/removal rate.

GRC's separator accomplishes the task of water removal by coupling a high aspect-ratio flow chamber with a highly hydrophilic, polyethersulfone membrane. The hydrophilic membrane readily absorbs and transports the liquid water away from the mixture while simultaneously resisting gas penetration. The expansive flow path maximizes the interaction of the water particles with the membrane while

minimizing the overall gas flow restriction. In essence, each fluid takes its corresponding path of least resistance, and the two fluids are effectively separated.

The GRC fuel-cell water separator has a broad range of applications, including commercial hydrogen-air fuel cells currently being considered for power generation in automobiles.

*This work was done by Kenneth Alan Burke, Caleb Fisher, and Paul Newman of Glenn Research Center. Further information is contained in a TSP (see page 1).*

*Inquiries concerning rights for the commercial use of this invention should be addressed to NASA Glenn Research Center, Innovative Partnerships Office, Attn: Steve Fedor, Mail Stop 4-8, 21000 Brookpark Road, Cleveland, Ohio 44135. Refer to LEW-18304-1.*





## Turbulence and the Stabilization Principle

NASA's Jet Propulsion Laboratory, Pasadena, California

Further results of research, reported in several previous *NASA Tech Briefs* articles, were obtained on a mathematical formalism for postinstability motions of a dynamical system characterized by exponential divergences of trajectories leading to chaos (including turbulence).

To recapitulate: Fictitious control forces are introduced to couple the dynamical equations with a Liouville equation that describes the evolution of the probability density of errors in initial conditions. These forces create a powerful terminal attractor in probabil-

ity space that corresponds to occurrence of a target trajectory with probability one. The effect in ordinary perceived three-dimensional space is to suppress exponential divergences of neighboring trajectories without affecting the target trajectory. Consequently, the postinstability motion is represented by a set of functions describing the evolution of such statistical quantities as expectations and higher moments, and this representation is stable.

The previously reported findings are analyzed from the perspective of the

authors' Stabilization Principle, according to which (1) stability is recognized as an attribute of mathematical formalism rather than of underlying physics and (2) a dynamical system that appears unstable when modeled by differentiable functions only can be rendered stable by modifying the dynamical equations to incorporate intrinsic stochasticity.

*This work was done by Michail Zak of Caltech for NASA's Jet Propulsion Laboratory. For more information, contact [iaoffice@jpl.nasa.gov](mailto:iaoffice@jpl.nasa.gov). NPO-45937*

## Improved Cloud Condensation Nucleus Spectrometer

**Droplets can be sampled over a wide range of supersaturations in a short time.**

NASA's Jet Propulsion Laboratory, Pasadena, California

An improved thermal-gradient cloud condensation nucleus spectrometer (CCNS) has been designed to provide several enhancements over prior thermal-gradient counters, including fast response and high-sensitivity detection covering a wide range of supersatura-

tions. CCNSs are used in laboratory research on the relationships among aerosols, supersaturation of air, and the formation of clouds. The operational characteristics of prior counters are such that it takes long times to determine aerosol critical supersaturations. Hence,

there is a need for a CCNS capable of rapid scanning through a wide range of supersaturations. The present improved CCNS satisfies this need.

The improved thermal-gradient CCNS (see Figure 1) incorporates the following notable features:

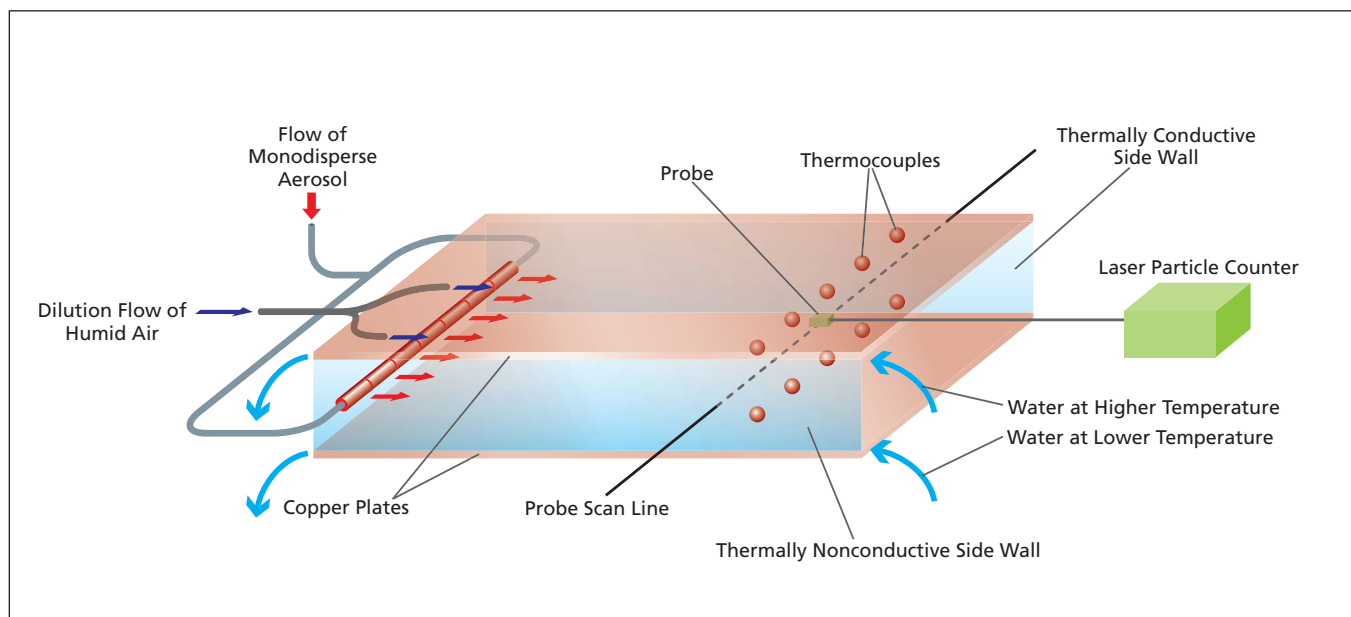


Figure 1. In the Improved Thermal-Gradient CCNS, a gradient supersaturation field is established in the main chamber. The probe is moved along the width axis to sample droplets over a range of supersaturations.

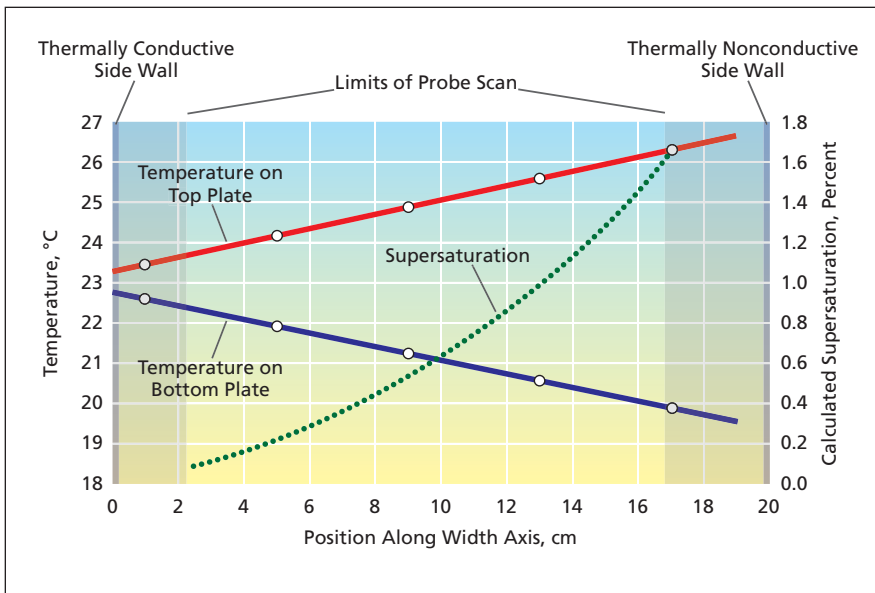


Figure 2. Straight-Line Fits to Temperature Readings of top- and bottom-plate thermocouples were used to calculate the supersaturation as a function of position along the width axis of the chamber.

- The main chamber is bounded on the top and bottom by parallel thick copper plates, which are joined by a thermally conductive vertical wall on one side and a thermally nonconductive wall on the opposite side.
- To establish a temperature gradient needed to establish a supersaturation gradient, water at two different regulated temperatures is pumped through tubes along the edges of the copper plates at the thermally-nonconductive-wall side. Figure 2 presents an example of temperature and supersaturation gradients for one combination of regulated tempera-

tures at the thermally-nonconductive-wall edges of the copper plates.

- To enable measurement of the temperature gradient, ten thermocouples are cemented to the external surfaces of the copper plates (five on the top plate and five on the bottom plate), spaced at equal intervals along the width axis of the main chamber near the outlet end.
- Pieces of filter paper or cotton felt are cemented onto the interior surfaces of the copper plates and, prior to each experimental run, are saturated with water to establish a supersaturation field inside the main chamber.

- A flow of monodisperse aerosol and a dilution flow of humid air are introduced into the main chamber at the inlet end. The inlet assembly is designed to offer improved (relative to prior such assemblies) laminar-flow performance within the main chamber. Dry aerosols are subjected to activation and growth in the supersaturation field.
- After aerosol activation, at the outlet end of the main chamber, a polished stainless-steel probe is used to sample droplets into a laser particle counter. The probe features an improved design for efficient sampling. The counter has six channels with size bins in the range of 0.5- to 5.0- $\mu\text{m}$  diameter.
- To enable efficient sampling, the probe is scanned along the width axis of the main chamber (thereby effecting scanning along the temperature gradient and thereby, further, effecting scanning along the supersaturation gradient) by means of a computer-controlled translation stage.

*This work was done by Ming-Taun Leu of Caltech for NASA's Jet Propulsion Laboratory.*

*In accordance with Public Law 96-517, the contractor has elected to retain title to this invention. Inquiries concerning rights for its commercial use should be addressed to:*

*Innovative Technology Assets Management  
JPL*

*Mail Stop 202-233*

*4800 Oak Grove Drive*

*Pasadena, CA 91109-8099*

*E-mail: iaoffice@jpl.nasa.gov*

*Refer to NPO-44761, volume and number of this NASA Tech Briefs issue, and the page number.*

## Better Modeling of Electrostatic Discharge in an Insulator

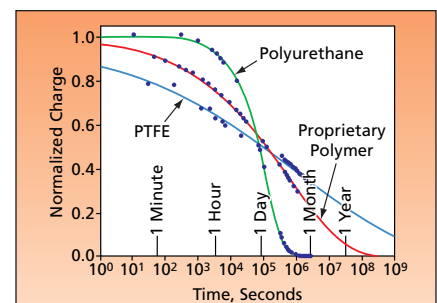
A model based on Kohlrausch relaxation gives improved fits to experimental data.

NASA's Jet Propulsion Laboratory, Pasadena, California

An improved mathematical model has been developed of the time dependence of buildup or decay of electric charge in a high-resistivity (nominally insulating) material. The model is intended primarily for use in extracting the DC electrical resistivity of such a material from voltage-vs.-current measurements performed repeatedly on a sample of the material over a time comparable to the longest characteristic times (typically of the order of months) that govern the evolution of relevant properties of the material. This model is an alternative to a prior simplistic macroscopic model that yields results

differing from the results of the time-dependent measurements by two to three orders of magnitude.

The present model is based on the Kohlrausch relaxation law, named after its author, who first reported a long-lasting dielectric relaxation in 1854. Since then, the Kohlrausch law has been used to describe a myriad of physical phenomena. Kohlrausch relaxation is also known as stretched exponential relaxation because the time-dependent value of a Kohlrausch-relaxing quantity of interest is proportional to the stretched exponential function  $\exp[-(t/\tau)^\beta]$



Kohlrausch Fits (the solid curves) were made to normalized-charge data calculated from long-term measurements on three different dielectrics: a poly(tetrafluoroethylene) [PTFE], a polyurethane, and a proprietary polymer.

where  $t$  is time,  $\tau$  is a characteristic relaxation time of the material in question, and  $\beta$  is a parameter (sometimes denoted the Kohlrausch exponent) that has a value between 0 and 1. Many microscopic models of transport in distributed systems (e.g., electron hopping, dipole fluctuation) have shown to result in Kohlrausch dependences of macroscopic observables.

In general, whichever model is used, the DC electrical resistivity of a material sample subjected to long-term charge-decay measurements is calculated from parameters used to fit the model to the measurement data. Various methods that

have been used to fit simplistic macroscopic models to measurement data involve large numbers of fitting parameters and involve user-dependent fitting calculations. In contrast, the Kohlrausch-relaxation-based model involves the minimum possible number of fitting parameters, and the associated fitting calculations are not user-dependent.

The applicability of the present model and its superiority to the prior macroscopic model have been demonstrated through the closeness with which this model has been shown to fit experimental data on normalized charge over 5 to 6 orders of magnitude in time (for exam-

ple, see figure). Although the validity of DC-resistivity values derived from fitting parameters of this model has yet to be demonstrated, the mere fact that these resistivity values differ from those obtained by application of the prior macroscopic model to the same experimental data indicates the need for further research to answer the questions of what are the relevant properties of the affected materials and what are the proper methods of determining these properties.

*This work was done by Mihail Petkov of Caltech for NASA's Jet Propulsion Laboratory. For more information, contact iaoffice@jpl.nasa.gov. NPO-44868*

## Sub-Aperture Interferometers

**Multiple target sub-beams are derived from the same measurement beam.**

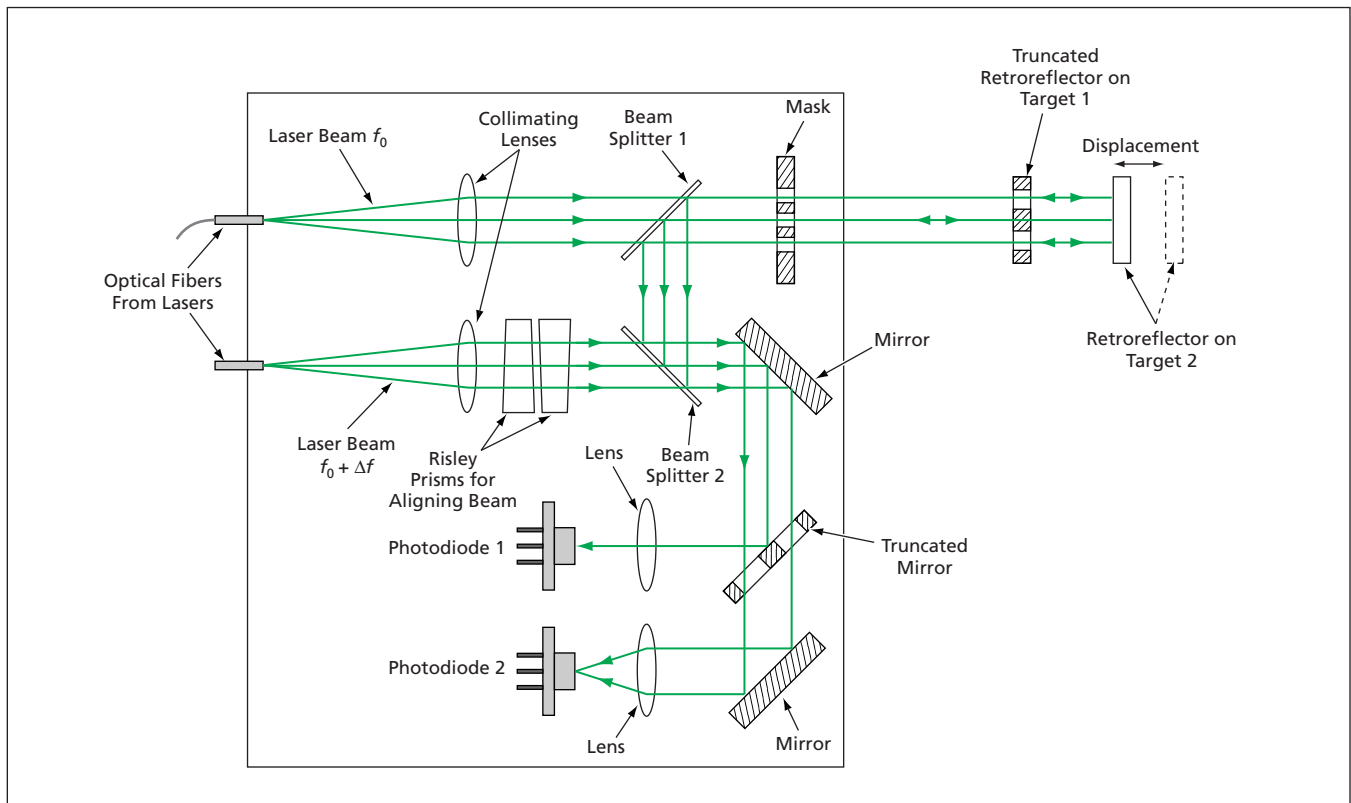
*NASA's Jet Propulsion Laboratory, Pasadena, California*

Sub-aperture interferometers — also called wavefront-split interferometers — have been developed for simultaneously measuring displacements of multiple targets. The terms “sub-aperture” and “wavefront-split” signify that the original measurement light beam in an

interferometer is split into multiple sub-beams derived from non-overlapping portions of the original measurement-beam aperture. Each measurement sub-beam is aimed at a retroreflector mounted on one of the targets. The splitting of the measure-

ment beam is accomplished by use of truncated mirrors and masks, as shown in the example below.

Sub-aperture interferometers incorporate some of the innovations described in two previous *NASA Tech Briefs* articles: “Common-Path Heter-



In this **Wavefront-Split Interferometer**, the truncated retroreflector on the first target and the retroreflector on the second target form a measurement optical cavity. The roles played by the measurement and reference beams in a typical prior interferometer are here played by two measurement sub-beams derived from the same measurement beam without use of extra optics.

odyne Interferometers” (NPO-20786), Vol. 25, No. 7 (July 2001), page 12a. and “Interferometer for Measuring Displacement to Within 20 pm” (NPO-21221), Vol. 27, No. 7 (July 2003), page 8a. Wavefront splitting is one of those innovations. To recapitulate from the second-mentioned article: Heretofore, the most popular method of displacement-measuring interferometry has involved two beams, the polarizations of which are meant to be kept orthogonal upstream of the final interference location, where the difference between the phases of the two beams is measured. Polarization leakage (deviations from the desired perfect orthogonality) contaminates the phase measurement with cyclic nonlinear errors. The advantage afforded by wavefront splitting arises from the fact that one does not utilize polarization in the separation and combination of the interfering beams; the cyclic nonlinear errors are much smaller because the polarization-leakage contribution is eliminated.

One example of a sub-aperture interferometer, denoted a sub-aperture vertex-to-vertex interferometer, is one of several prototype common-path heterodyne interferometers designed and built at NASA’s Jet Propulsion Laboratory. This interferometer (see figure) makes use of two collimated laser beams — one at a frequency of  $f_0$ , the other at the slightly different frequency of  $f_0 + \Delta f$ . The  $f_0$  beam is denoted the measurement beam. It passes through beam splitter 1 on its way toward two targets. The retroreflector on the first target is truncated; it is a flat mirror that reflects a portion of the measurement beam and contains two holes through which portions of the measurement beam continue toward the second target and through which they return after reflection from the retroreflector on the second target. A mask establishes guard bands between the measurement sub-beams to reduce diffraction.

The measurement sub-beams returning from the targets are reflected from beam splitter 1 to beam splitter 2,

where the  $f_0 + \Delta f$  beam becomes superimposed upon them. Then by use of mirrors (one of which is truncated) and lenses, the  $f_0$  sub-beam from target 1 and part of the  $f_0 + \Delta f$  beam are sent to photodiode 1 while the  $f_0$  sub-beam from target 2 and another part of the  $f_0 + \Delta f$  beam are sent to photodiode 2. The lowest-frequency components of the heterodyne outputs of the two photodetectors are signals of frequency  $\Delta f$ . The difference between the phases of these heterodyne signals is proportional to the difference between the lengths of the optical paths to the two target retroreflectors. Any displacement of either target along the optical path results in a proportional change in this phase difference. Hence, measurement of the phase difference and of any change in the phase difference yields information on the displacement.

*This work was done by Feng Zhao of Caltech for NASA’s Jet Propulsion Laboratory. For more information, contact [iaoffice@jpl.nasa.gov](mailto:iaoffice@jpl.nasa.gov). NPO-30779*

## Terahertz Mapping of Microstructure and Thickness Variations

**Previously, it was not possible to separate microstructural and thickness effects using electromagnetic methods.**

*John H. Glenn Research Center, Cleveland, Ohio*

A noncontact method has been devised for mapping or imaging spatial variations in the thickness and microstructure of a layer of a dielectric material. The method involves (1) placement of the dielectric material on a metal substrate, (2) through-the-thickness pulse-echo measurements by use of electromagnetic waves in the terahertz frequency range with a raster scan in a plane parallel to the substrate surface that do not require coupling of any kind, and (3) appropriate processing of the digitized measurement data.

More specifically, the method provides for mapping, in a coordinate system defined by the raster scan, of spatial variations of the thickness normal to the substrate surface and spatial variations of the through-the-thickness velocity of the terahertz mapping signal. (In general, variations in the velocity of this or any signal through a material are associated with variations in density and/or other characteristics associated with local microstructure of the material.) The method has been demonstrated on

nominally flat metal-backed specimens of two dielectric materials: a silicon nitride ceramic and a spray-on foam of the type used on the external tanks of a space shuttle. The method should also be applicable to other dielectric materials, and it may be feasible to extend the method to cylindrical, beveled, and other non-planar shapes.

In a prior method of terahertz mapping or imaging of this type as applied to space-shuttle external-tank foam bonded to the metal tank surface, one maps variations in the time of flight of the terahertz signal through the thickness of the foam, the time of flight being typically defined as the time between the echo from the substrate surface and the front foam surface. That approach yields information on the combined effects of thickness and through-the-thickness velocity; it does not enable separate determination of variations in thickness and variations in velocity.

In contrast, the present method provides for generation of velocity-variation images free of thickness-variation effects

and thickness-variation images free of velocity-variation effects. In this method, terahertz pulse-echo measurements with a raster scan are made as in the prior method. The raster-scan plane is chosen so that there is a suitable air gap between the terahertz transceiver and the front surface of the dielectric material. One difference between the present and prior methods is that two sets of data are acquired: For one set, the sample is absent and the times of the echoes from the substrate alone are measured. For the other set, the dielectric sample is placed on the metal substrate and echoes from both the substrate and front surface of the dielectric are measured as in the prior method.

Another difference between the present and prior methods lies in processing of the two sets of measurement data. The processing is effected by special-purpose software that performs signal-enhancement and data-fusion functions to obtain enhanced values of the times of front-surface and substrate echoes in the presence of the dielectric sample



and of the substrate echo in the absence of the sample. Then by use of equations that are readily derived from the basic signal time-of-flight equations, the thickness of the sample and the through-the-thickness velocity in the sample are com-

puted from the various echo times.

*This work was done by Donald J. Roth, Jeffrey P. Seebo, and William P. Winfree of Glenn Research Center. Further information is contained in a TSP (see page 1).*

*Inquiries concerning rights for the*

*commercial use of this invention should be addressed to NASA Glenn Research Center, Innovative Partnerships Office, Attn: Steve Fedor, Mail Stop 4-8, 21000 Brookpark Road, Cleveland, Ohio 44135. Refer to LEW-18254-1.*

---

## Multiparallel Three-Dimensional Optical Microscopy

*Lyndon B. Johnson Space Center, Houston, Texas*

Multiparallel three-dimensional optical microscopy is a method of forming an approximate three-dimensional image of a microscope sample as a collection of images from different depths through the sample. The imaging apparatus includes a single microscope plus an assembly of beam splitters and mirrors that divide the output of the microscope into multiple channels. An imaging array of photodetectors in each channel is located at a different distance along the optical path from the microscope, corresponding to a focal plane at a different depth within the sample. The optical path leading to each photodetector array also includes lenses to compen-

sate for the variation of magnification with distance so that the images ultimately formed on all the photodetector arrays are of the same magnification.

The use of optical components common to multiple channels in a simple geometry makes it possible to obtain high light-transmission efficiency with an optically and mechanically simple assembly. In addition, because images can be read out simultaneously from all the photodetector arrays, the apparatus can support three-dimensional imaging at a high scanning rate.

*This work was done by Lam K. Nguyen, Jeffrey H. Price, Albert L. Kellner, and Miguel Bravo-Zanoquera of the University of Califor-*

*nia for Johnson Space Center. For further information, contact the JSC Innovation Partnerships Office at (281) 483-3809.*

*In accordance with Public Law 96-517, the contractor has elected to retain title to this invention. Inquiries concerning rights for its commercial use should be addressed to:*

*University of California, San Diego  
Technology Transfer and Intellectual  
Property Services*

*9500 Gilman Drive, Dept. 0910*

*La Jolla, CA 92093-0910*

*Phone No.: (858) 534-5815*

*Fax No.: (858) 534-7345*

*Refer to MSC-23851-1, volume and number of this NASA Tech Briefs issue, and the page number.*

---

## Stabilization of Phase of a Sinusoidal Signal Transmitted Over Optical Fiber

**Two-way transmissions allow for rapid correction of common reference tones.**

*NASA's Jet Propulsion Laboratory, Pasadena, California*

In the process of connecting widely distributed antennas into a coherent array, it is necessary to synchronize the timing of signals at the various locations. This can be accomplished by distributing a common reference signal from a central source, usually over optical fiber. A high-frequency (RF or microwave) tone is a good choice for the reference. One difficulty is that the effective length of the optical fiber changes with temperature and mechanical stress, leading to phase instability in the received tone. This innovation provides a new way to stabilize the phase of the received tone, in spite of variations in the electrical length of the fiber.

Stabilization is accomplished by two-way transmission in which part of the received signal is returned to the transmitting end over an identical fiber. The returned signal is detected and used to

close an electrical servo loop whose effect is to keep constant the phase of the tone at the receiving end.

The technique is useful in large arrays of Earth-based antennas used for space communication or radio astronomy. It is also useful in any situation where precise timing information must be transferred over distances for which optical fiber transmission is appropriate (~10 m to 30 km). It has been used in a demonstration uplink array as part of a technology development for the Deep Space Network.

In the past, other techniques have been used for a similar purpose, but they involve either manipulation of the optical fibers, or they measure and record the phase variation rather than correcting it immediately via a closed-loop servo. The optical methods are generally slow, so they cannot correct

rapid variations. The open-loop methods are less accurate, and they are not useful in situations where real-time correction is needed. The method described here is fast, accurate, and inexpensive to implement. A method similar in principle to this one has been reported earlier, but the new configuration is different and permits variable transmitted frequency and higher correction speed. Related round-trip stabilization methods have been used for signal transmission in coaxial cable and in waveguide

The new method is illustrated by the block diagram in Figure 1. The signal to be transmitted is at frequency  $f_0$ . It is generated by mixing an input at  $f_0 + f_1$  (from the first master synthesizer) with a voltage-controlled crystal oscillator (VCXO) at nominal frequency  $f_1$  (77.76 MHz in this implementation). It

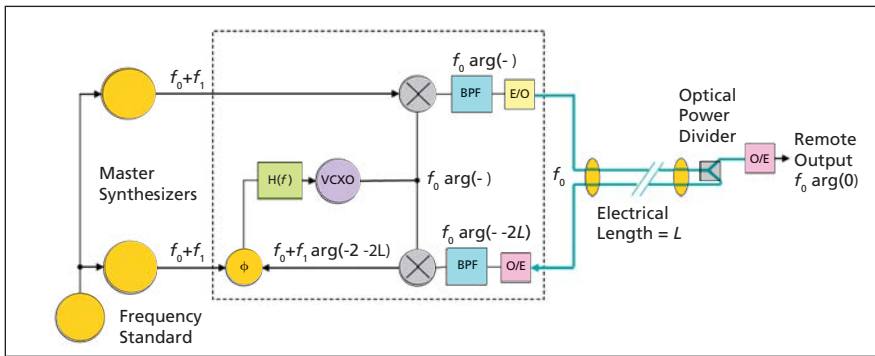


Figure 1: **Simplified Block Diagram** of the phase stabilization system, showing its principle of operation. Components in the dashed box form the reference generator module. Here E/O and O/E denote electrical-to-optical conversion (laser) and optical-to-electrical conversion (photodetector), respectively, and BPF denotes a band-pass filter. Changes in line length  $L$  are compensated by a phase-locked loop driving a voltage-controlled crystal oscillator. In this implementation, the VCXO frequency is  $f_1 = 77.76$  MHz, and the output frequency  $f_0$  is in the range 437 to 454 MHz.

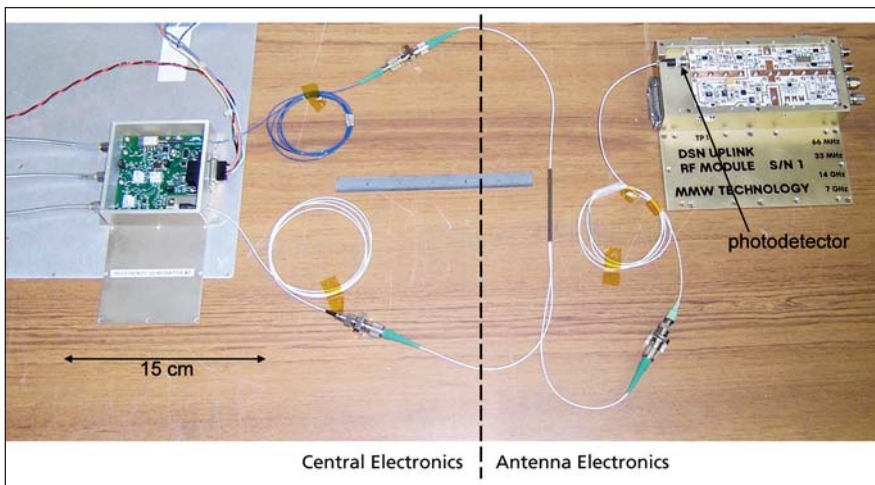


Figure 2: **System Undergoing Laboratory** testing is shown with short fiber connections. The Reference Generator Module is the 5x5 cm box at the left. It includes the laser and photodetector for electrical/optical conversion. The blue fiber at the top carries the outgoing signal and the white fiber at the bottom carries the returned signal. At the right is equipment intended for installation at the remote location, including an optical power divider and a module that includes the photodetector along with circuitry for this application that uses the output signal.

is then used to modulate a diode laser coupled to the outgoing fiber. At the far end of the fiber, the signal is optically split and half of its power is converted back to electrical form in a photodetector, producing the desired output. The other half is returned to the stabilization system over a nominally-identical fiber in the same cable. The returned signal is converted to electrical form, then down-converted in frequency by mixing with the same VCXO, and the result is compared in phase against an input from the second master synthesizer at  $f_0 - f_1$ . The phase difference is used to drive the frequency of the VCXO via filter  $H(f)$ , forming a phase-locked loop. If the input signals are considered to have phase zero, it is easy to show that the loop will drive the phase  $\theta$  of the VCXO so that  $2\theta = (2L) \bmod 2\pi$ , where

$L$  is the electrical length of the line in each direction, causing the phase of the signal at the turn-around point to remain constant as  $L$  is changed. The actual phase there has a two-fold ambiguity; it could be either 0 or  $\pi$ . (These expressions neglect delays in the electronics, but those cancel if they are equal in the two directions. If they are unequal but stable, the output phase remains stable even though the electrical length of the fiber varies.) The important assumption is that the variation in fiber electrical length is the same in the two directions.

The system can be used to generate coherent signals at multiple remote locations by duplicating the assembly labeled Reference Generator Module (RGM) in Figure 1 and driving all RGMs with the same master synthesizer signals. If all RGMs and photodetectors are iden-

tical, and if each pair of fibers is reciprocal (same electrical length in both directions), then the output signals at all remote locations have equal phase, even if the fiber pairs to the various locations have vastly different lengths.

This system has an advantage over those that rely on manipulation of the fiber because it can correct variations in the fiber length much faster. In some applications, the dominant cause of changes in fiber length is temperature variation, but there are also circumstances where the fiber is subject to varying mechanical stress, such as when it must traverse the rotation axes of a movable reflector antenna. Temperature changes are often slow (and can be further slowed by adding insulation), but mechanical changes can be rapid. Here the correction speed is limited only by the round-trip signal time; for the loop to be stable, it must have a time constant at least several times the round-trip time.

It is also possible to vary the transmitted frequency  $f_0$  while maintaining constant phase differences among multiple remote locations. The rate of frequency change need only be slow enough that all of the correction loops remain phase locked.

This system was implemented for operation in the range  $f_0 = 437$  to 454 MHz and was used to provide coherent reference signals to the antennas of a 5-element microwave phased array. In this frequency range, the RGM can be made small and inexpensive, as shown in Figure 2. Before deploying it in the array, the innovators conducted tests using a 305-m long spool of multi-fiber cable where both ends of the cable were in the laboratory so that the input and output phases could be compared. The spool was kept outdoors and subjected to diurnal temperature cycling over several days. With the correction loop disabled, phase changes of  $26.5^\circ$  peak-to-peak were observed at 450 MHz with  $23.9^\circ\text{C}$  peak-to-peak temperature change; this corresponds to a delay coefficient of  $6.2$  ps/ $^\circ\text{C}$ , which is about as expected for this length of standard single-mode fiber. With the correction loop enabled, no variation with fiber temperature was detectable, and the measurements placed an upper limit on the coefficient of  $0.054$  ps/ $^\circ\text{C}$ .

*This work was done by Larry R. D'Addario and Joseph T. Trinh of Caltech for NASA's Jet Propulsion Laboratory. Further information is contained in a TSP (see page 1). NPO-46711.*

# Vacuum-Compatible Wideband White Light and Laser Combiner Source System

NASA's Jet Propulsion Laboratory, Pasadena, California

For the Space Interferometry Mission (SIM) Spectrum Calibration Development Unit (SCDU) testbed, wideband white light is used to simulate starlight. The white light source mount requires extremely stable pointing accuracy ( $<3.2$  microradians). To meet this and other needs, the laser light from a single-mode fiber was combined, through a beam splitter window with special coating from broadband wavelengths, with light from multimode fiber. Both lights were coupled to a photonic crystal fiber (PCF).

In many optical systems, simulating a point star with broadband spectrum with stability of microradians for white light interferometry is a challenge. In this case, the cameras use the white light interference to balance two optical paths, and to maintain close tracking. In order

to coarse align the optical paths, a laser light is sent into the system to allow tracking of fringes because a narrow band laser has a great range of interference.

The design requirements forced the innovators to use a new type of optical fiber, and to take a large amount of care in aligning the input sources. The testbed required better than 1% throughput, or enough output power on the lowest spectrum to be detectable by the CCD camera (6 nW at camera). The system needed to be vacuum-compatible and to have the capability for combining a visible laser light at any time for calibration purposes.

The red laser is a commercially produced 635-nm laser 5-mW diode, and the white light source is a commercially produced tungsten halogen lamp that

gives a broad spectrum of about 525 to 800 nm full width at half maximum (FWHM), with about 1.4 mW of power at 630 nm. A custom-made beam splitter window with special coating for broadband wavelengths is used with the white light input via a 50-mm multi-mode fiber. The large mode area PCF is an LMA-8 made by Crystal Fibre (core diameter of 8.5 mm, mode field diameter of 6 mm, and numerical aperture at 625 nm of 0.083). Any science interferometer that needs a tracking laser fringe to assist in alignment can use this system.

*This work was done by Alireza Azizi, Daniel J. Ryan, Hong Tang, Richard T. Demers, Hiroshi Kadogawa, Xin An, and George Y. Sun of Caltech for NASA's Jet Propulsion Laboratory. Further information is contained in a TSP (see page 1). NPO-46165*

# Optical Tapers as White-Light WGM Resonators

**Such resonators could be attractive for broad-band optical processing applications.**

NASA's Jet Propulsion Laboratory, Pasadena, California

A theoretical analysis has revealed that tapered optical waveguides could be useful as white-light whispering-gallery-mode (WGM) optical resonators. The compactness and the fixed-narrow-frequency-band nature of the resonances of prior microdisk and microsphere WGM resonators are advantageous in low-power, fixed-narrow-frequency-band applications. However for optical-processing applications in which there are requirements for power levels higher and/or spectral responses broader than those of prior microdisk and microsphere WGM resonators, white-light WGM resonators in the form of optical tapers would be preferable.

In a typical prior microdisk or microsphere WGM resonator, the optical power is concentrated mostly in a small WGM volume, making it necessary to limit the power to a low level in order to minimize undesired nonlinear optical and thermo-optical effects. If one could construct a WGM resonator in which the optical power were spread over a larger volume, then the threshold power level for the onset of undesired nonlinear optical and thermo-optical effects would be higher.

The theoretical analysis was performed for a multimode, axisymmetric, circular-cross-section waveguide having a taper sufficiently smooth and gradual to justify the approximation of adiabaticity. In this approximation, the equation for the dependence of the electromagnetic field upon the axial (longitudinal) waveguide coordinate ( $z$ ) can be separated from the equation for the dependence upon the radius ( $r$ ) and the azimuthal angle ( $\phi$ ). Electromagnetic modes characterized by high angular momentum (equivalently, large values of the  $\phi$ -dependence quantum number) were considered. The solution of the equation for the axial dependence was found to be an amplitude that varies gradually with  $z$ . For a given axial location  $z$ , where the outer surface of the waveguide has a radius  $R(z)$ , the solutions for the radial and azimuthal dependences were found to be WGM modes equivalent to those for a cylinder of radius  $R(z)$ .

In effect, it was found that the tapered waveguide can be considered to support WGMs propagating along the waveguide axis. It was further found that as the radius tapers down toward the classical

critical radius  $R_c$  at a classical turn-around axial position  $z_c$ , the group delay of a WGM increases and the electromagnetic field becomes increasingly concentrated, albeit in an effective mode volume typically much larger than the mode volume in a prior microdisk or microsphere WGM resonator. Thus, it was found that the power density of the electromagnetic field is much less than in a prior microdisk or microsphere WGM resonator and the onset of undesired nonlinearities is shifted to a significantly higher power level. It was found that in the special case of a linear taper, the turning point varies linearly with the frequency of the electromagnetic field, while the resonance quality factor and dispersion remain fixed to first order.

A resonator having these characteristics can be considered a white-light resonator in that it exhibits resonance over a continuous frequency range.

*This work was done by Dmitry V. Strelakov and Andrey B. Matsko of Caltech and Anatoliy A. Savchenkov of OE Waves for NASA's Jet Propulsion Laboratory. For more information, contact [iaoffice@jpl.nasa.gov](mailto:iaoffice@jpl.nasa.gov). NPO-45842*

## EPR Imaging at a Few Megahertz Using SQUID Detectors

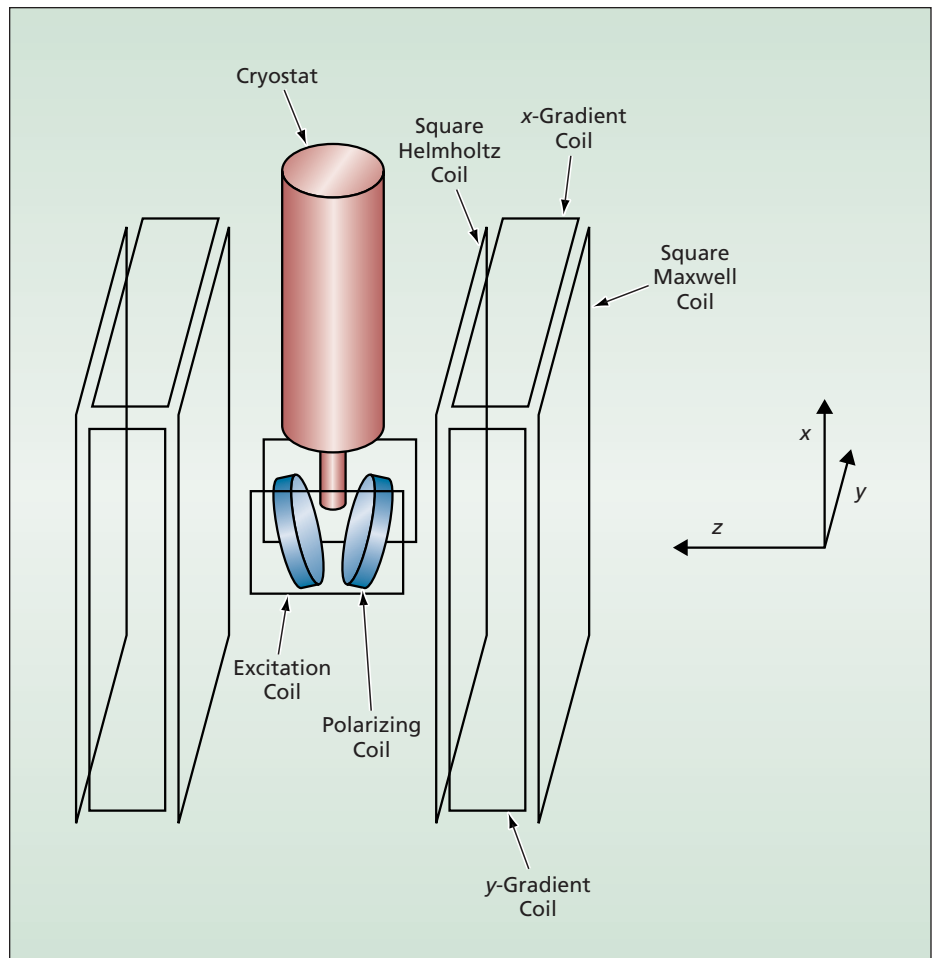
This frequency range is better for imaging of humans and large animals.

NASA's Jet Propulsion Laboratory, Pasadena, California

An apparatus being developed for electron paramagnetic resonance (EPR) imaging operates in the resonance-frequency range of about 1 to 2 MHz — well below the microwave frequencies used in conventional EPR. Until now, in order to obtain sufficient signal-to-noise ratios (SNRs) in conventional EPR, it has been necessary to place both detectors and objects to be imaged inside resonant microwave cavities.

EPR imaging has much in common with magnetic resonance imaging (MRI), which is described briefly in the immediately preceding article. In EPR imaging as in MRI, one applies a magnetic pulse to make magnetic moments (in this case, of electrons) precess in an applied magnetic field having a known gradient. The magnetic moments precess at a resonance frequency proportional to the strength of the local magnetic field. One detects the decaying resonance-frequency magnetic-field component associated with the precession. Position is encoded by use of the known relationship between the resonance frequency and the position dependence of the magnetic field.

EPR imaging has recently been recognized as an important tool for non-invasive, *in vivo* imaging of free radicals and reduction/oxidization metabolism. However, for *in vivo* EPR imaging of humans and large animals, the conventional approach is not suitable because (1) it is difficult to design and construct resonant cavities large enough and having the required shapes; (2) motion, including respiration and heartbeat, can alter the resonance frequency; and (3) most microwave energy is absorbed in the first few centimeters of tissue depth, thereby potentially endangering the subject and making it impossible to obtain adequate signal strength for imaging at greater depth. To obtain greater penetration depth, prevent injury to the subject, and avoid the difficulties associated with resonant cavities, it is necessary to use lower resonance frequencies. An additional advantage of using lower resonance frequencies is that one can use weaker mag-



The Electromagnet Coils and the Cryostat of the present SQUID EPR imaging apparatus are depicted here in simplified form.

netic fields: For example, for a resonance frequency of 1.4 MHz, one needs a magnetic flux density of 0.5 Gauss — approximately the flux density of the natural magnetic field of the Earth.

In the present apparatus, a superconducting quantum interference device (SQUID) is used in detecting the EPR signal. Even without a cavity resonator, in the frequency range of about 1 to 2 MHz, it is possible to obtain a sufficient SNR by use of a simple pickup coil placed near the surface of the object to be imaged. The pickup coil is part of a flux transformer coupled to the SQUID. The signal is detected by either a commercial SQUID array amplifier device (which has a typical bandwidth of about 1 MHz) or a custom microwave SQUID (which has a typical bandwidth of about 10 MHz). To increase the SNR, the out-

put of the microwave SQUID can be fed to a cryogenic high-electron-mobility transistor amplifier.

The figure depicts the layout of the electromagnetic coils and the cryostat (which houses the SQUID circuitry) of the present apparatus. These coils are identical to those of a low-magnetic-field-strength SQUID MRI apparatus developed in the same laboratory. In one mode of operation, the polarizing coils are used to prepolarize the specimen by applying a magnetic field stronger than the nearly homogeneous magnetic field generated by the Helmholtz coils; the prepolarizing field is then rapidly turned off immediately before starting to record EPR imaging data. The polarizing coils are positioned and oriented so as not to induce measurable flux in the pickup coil. It is important to note

that in some cases, the EPR signal may be strong enough to be detectable even in the absence of prepolarization.

*This work was done by Inseob Hahn, Peter Day, Konstantin Penanen, and Byeong Ho Eom of Caltech and Mark Cohen of UCLA Center for Cognitive Neuroscience for NASA's*

*Jet Propulsion Laboratory.*

*In accordance with Public Law 96-517, the contractor has elected to retain title to this invention. Inquiries concerning rights for its commercial use should be addressed to:*

*Innovative Technology Assets Management  
JPL*

*Mail Stop 202-233*

*4800 Oak Grove Drive*

*Pasadena, CA 91109-8099*

*E-mail: iaoffice@jpl.nasa.gov*

*Refer to NPO-44656, volume and number of this NASA Tech Briefs issue, and the page number.*

## Reducing Field Distortion in Magnetic Resonance Imaging

An unconventional magnetic-field configuration would be used in SQUID MRI.

NASA's Jet Propulsion Laboratory, Pasadena, California

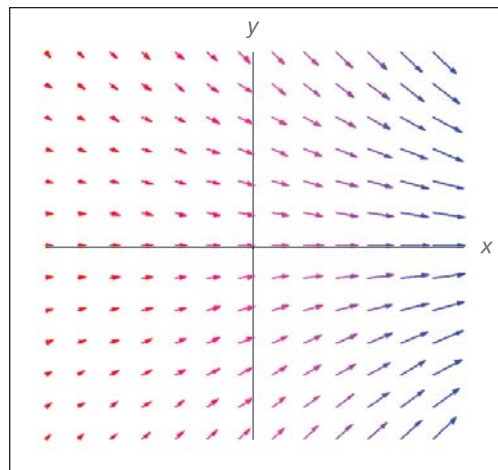
A concept for a magnetic resonance imaging (MRI) system that would utilize a relatively weak magnetic field provides for several design features that differ significantly from the corresponding features of conventional MRI systems. Notable among these features are a magnetic-field configuration that reduces (relative to the conventional configuration) distortion and blurring of the image, the use of a superconducting quantum interference device (SQUID) magnetometer as the detector, and an imaging procedure suited for the unconventional field configuration and sensor.

In a typical application of MRI, a radio-frequency pulse is used to excite precession of the magnetic moments of protons in an applied magnetic field, and the decaying precession is detected for a short time following the pulse. The precession occurs at a resonance frequency proportional to the strengths of the magnetic field and the proton magnetic moment. The magnetic field is configured to vary with position in a known way; hence, by virtue of the aforesaid proportionality, the resonance frequency varies with position in a known way. In other words, position is encoded as resonance frequency.

MRI using magnetic fields weaker than those of conventional MRI offers several advantages, including cheaper and smaller equipment, greater compatibility with metallic objects, and higher image quality because of low susceptibility distortion and enhanced spin-lattice-relaxation-time contrast. SQUID MRI is being developed into a practical MRI method for applied magnetic flux densities of the order of only 100  $\mu$ T.

In conventional MRI, it is required that all of the magnetic moments precess around the same axis defined by an applied static, homogeneous magnetic

field. One of the problems in developing low-magnetic-field-strength MRI arises from the relationship among image resolution, image-acquisition time, and the gradient of the magnetic field. In general, the resolution (that is, the reciprocal of the smallest size of an



Field Configuration is shown in  $x,y$  plane.

image feature that can be resolved) is proportional to the strength of the magnetic-field gradient and the image-acquisition time. Because of fundamental properties of a magnetic field, an image-position-encoding gradient necessarily entails undesired concomitant field components proportional to the image-position-encoding gradient. These components are undesired because they cause distortion or blurring of the image. The distortion can be reduced by weakening the gradient so that the total field variation in the magnetic field is a small fraction of the static homogeneous field. However, in weakening the gradient, one must either accept lower resolution or else increase image-acquisition time to retain resolution.

According to the present concept, it should be possible to reduce distortion to a very low (in principle, negligible)

level while using a low-strength magnetic field, without sacrificing resolution and without need for excessively long image-acquisition time. There would be no applied static, homogeneous field because in MRI, it is not required that all the magnetic moments precess about the same axis. The encoding magnetic field,  $\mathbf{B}$ , would be configured to lie in the  $x,y$  plane of  $x,y,z$  Cartesian coordinate system: the field would be given by

$$\mathbf{B} = B_0 e^{x/a} [\hat{x} \cos(y/a) - \hat{y} \sin(y/a)]$$

where  $\hat{x}$  and  $\hat{y}$  are unit vectors along the  $x$  and  $y$  axes and  $B_0$  and  $a$  are arbitrary constants to be chosen by design (see figure). Inasmuch as the strength of this field is given by  $|\mathbf{B}| = B_0 e^{x/a}$ , this field would encode position along the  $x$  axis as a function of resonance frequency. Although  $x$  would be a nonlinear (specifically, a logarithmic) function of resonance frequency, it would be possible, through suitable choice of the arbitrary constants, to reduce the deviation from linearity and the concomitant spatial variation of resolution over the image region to tolerable levels.

A close approximation of the magnetic field described above could be generated by electric currents flowing axially on a  $z$ -oriented circular cylinder having a length much greater than its radius. The current density ( $K$ ) needed to generate the magnetic field is a known continuous function of the azimuthal angle ( $\theta$ ). In practice, the required continuous current density  $K(\theta)$  would be approximated by use of multiple discrete wires positioned at suitable angular intervals and driven by suitable currents. To encode position along an axis at an angle  $\alpha$  with respect to the  $x$  axis in the  $x,y$  plane so that back projection reconstruction could be used, one would shift the cur-

rent-density pattern by electronically changing the pattern of drive currents to make it approximate  $K(\theta + \alpha)$ .

In SQUID MRI, the magnetic moments are prepolarized in a strong magnetic field separate from the encoding field. In a system according to the present concept, the prepolarizing magnetic field would be oriented along the  $z$  axis. The prepolarizing magnetic would then be turned off so rapidly that immediately afterward, the magnetic moments would re-

main polarized and would start to precess about the  $x,y$ -oriented encoding magnetic field. The sensing loop of the SQUID magnetometer would be placed to detect the  $z$  component of magnetization.

*This work was done by Byeong Ho Eom, Konstantin Penanen, and Inseob Hahn of Caltech for NASA's Jet Propulsion Laboratory. Further information is contained in a TSP (see page 1).*

*In accordance with Public Law 96-517, the contractor has elected to retain title to this*

*invention. Inquiries concerning rights for its commercial use should be addressed to:*

*Innovative Technology Assets Management  
JPL*

*Mail Stop 202-233*

*4800 Oak Grove Drive*

*Pasadena, CA 91109-8099*

*E-mail: iaoffice@jpl.nasa.gov*

*Refer to NPO-44593, volume and number of this NASA Tech Briefs issue, and the page number.*



### **Fluorogenic Cell-Based Biosensors for Monitoring Microbes**

*Lyndon B. Johnson Space Center, Houston, Texas*

Fluorogenic cell-based sensor systems for detecting microbes (especially pathogenic ones) and some toxins and allergens are undergoing development. These systems harness the natural signal-transduction and amplification cascades that occur in mast cells upon activation with antigens. These systems include (1) fluidic biochips for automated containment of samples, reagents, and wastes and (2) sensitive, compact fluorometers for monitoring the fluorescent responses of mast cells engineered to contain fluorescent dyes. It should be possible to observe responses within minutes of adding immune complexes. The sys-

tems have been shown to work when utilizing either immunoglobulin E (IgE) antibodies or traditionally generated rat antibodies — a promising result in that it indicates that the systems could be developed to detect many target microbes. Chimeric IgE antibodies and rat immunoglobulin G (IgG) antibodies could be genetically engineered for recognizing biological and chemical warfare agents and airborne and food-borne allergens. Genetic engineering efforts thus far have yielded (1) CD14 chimeric antibodies that recognize both Gram-positive and Gram-negative bacteria and bind to the surfaces of mast cells, eliciting a degranulation response and (2) rat IgG2a antibodies that act similarly in response to low levels of canine parvovirus.

*This work was done by Theresa Curtis, Noe Salazar, Joel Tabb, and Chris Chase of Agave BioSystems for Johnson Space Center. For further information, contact the Johnson Commercial Technology Office at (281) 483-3809.*

*This invention is owned by NASA, and a patent application has been filed. Inquiries concerning nonexclusive or exclusive license for its commercial development should be addressed to the Patent Counsel, Johnson Space Center, (281) 483-1003. Refer to MSC-23797-1.*

### **A Constant-Force Resistive Exercise Unit**

*Lyndon B. Johnson Space Center, Houston, Texas*

A constant-force resistive exercise unit (CFREU) has been invented for use in both normal gravitational and microgravitational environments. In comparison with a typical conventional exercise machine, this CFREU weighs less and is less bulky: Whereas weight plates and associated bulky supporting structures are used to generate resistive forces in typical conventional exercise machines, they are not used in this CFREU. Instead, resistive forces are generated in this CFREU by relatively compact, lightweight mechanisms based on constant-torque

springs wound on drums. Each such mechanism is contained in a module, denoted a resistive pack, that includes a shaft for making a torque connection to a cable drum. During a stroke of resistive exercise, the cable is withdrawn from the cable drum against the torque exerted by the resistance pack.

The CFREU includes a housing, within which can be mounted one or more resistive pack(s). The CFREU also includes mechanisms for engaging any combination of (1) one or more resistive pack(s) and (2) one or more spring(s)

within each resistive pack to obtain a desired level of resistance.

*This work was done by Paul Colosky and Tara Ruttle of Valeo Human Systems, Inc., for Johnson Space Center.*

*In accordance with Public Law 96-517, the contractor has elected to retain title to this invention. Inquiries concerning rights for its commercial use should be addressed to:*

*Valeo Human Systems, Inc.  
3350 Eastbrook Dr., Ste. 109  
Fort Collins, CO 80525*

*Refer to MSC-23373-1, volume and number of this NASA Tech Briefs issue, and the page number.*

### **GUI To Facilitate Research on Biological Damage From Radiation**

*Lyndon B. Johnson Space Center, Houston, Texas*

A graphical-user-interface (GUI) computer program has been developed to facilitate research on the damage caused by highly energetic particles and photons impinging on living organisms. The program brings together, into one computational workspace, computer codes

that have been developed over the years, plus codes that will be developed during the foreseeable future, to address diverse aspects of radiation damage. These include codes that implement radiation-track models, codes for biophysical models of breakage of deoxyribonucleic acid

(DNA) by radiation, pattern-recognition programs for extracting quantitative information from biological assays, and image-processing programs that aid visualization of DNA breaks.

The radiation-track models are based on transport models of interactions of radia-

tion with matter and solution of the Boltzmann transport equation by use of both theoretical and numerical models. The biophysical models of breakage of DNA by radiation include biopolymer coarse-grained and atomistic models of DNA, stochastic-process models of deposition of en-

ergy, and Markov-based probabilistic models of placement of double-strand breaks in DNA. The program is designed for use in the NT, 95, 98, 2000, ME, and XP variants of the Windows operating system.

*This program was written by Frances A. Cucinotta of Johnson Space Center and Artem*

*Lvovich Ponomarev of Universities Space Research Association. Further information is contained in a TSP (see page 1).*

*Universities Space Research Association has requested permission to assert copyright for the software code. MSC-23853-1*

---

## On-Demand Urine Analyzer

*John H. Glenn Research Center, Cleveland, Ohio*

A lab-on-a-chip was developed that is capable of extracting biochemical indicators from urine samples and generating their surface-enhanced Raman spectra (SERS) so that the indicators can be quantified and identified. The development was motivated by the need to monitor and assess the effects of extended weightlessness, which include space motion sickness and loss of bone and muscle mass. The results may lead to developments of effective exercise

programs and drug regimes that would maintain astronaut health.

The analyzer containing the lab-on-a-chip includes materials to extract 3-methylhistidine (a muscle-loss indicator) and Risedronate (a bone-loss indicator) from the urine sample and detect them at the required concentrations using a Raman analyzer. The lab-on-a-chip has both an extractive material and a SERS-active material. The analyzer could be used to monitor the

onset of diseases, such as osteoporosis.

*This work was done by Stuart Farquharson, Frank Inscore, and Chetan Shende of Real-Time Analyzers, Inc. for Glenn Research Center. Further information is contained in a TSP (see page 1).*

*Inquiries concerning rights for the commercial use of this invention should be addressed to NASA Glenn Research Center, Innovative Partnerships Office, Attn: Steve Fedor, Mail Stop 4-8, 21000 Brookpark Road, Cleveland, Ohio 44135. Refer to LEW-18258-1.*

---

## More-Realistic Digital Modeling of a Human Body

*Lyndon B. Johnson Space Center, Houston, Texas*

A MATLAB computer program has been written to enable improved (relative to an older program) modeling of a human body for purposes of designing space suits and other hardware with which an astronaut must interact. The older program implements a kinematic

model based on traditional anthropometric measurements that do provide important volume and surface information. The present program generates a three-dimensional (3D) whole-body model from 3D body-scan data. The program utilizes thin-plate spline theory to

reposition the model without need for additional scans.

*This program was written by Renee Rogge of Mercer University for Johnson Space Center. For further information, contact the Johnson Commercial Technology Office at (281) 483-3809. MSC-24040-1*

---

## Advanced Liquid-Cooling Garment Using Highly Thermally Conductive Sheets

**This garment provides metabolic heat rejection applicable to surgical cooling vests, combat fatigues, and firefighter and hazmat suits.**

*Lyndon B. Johnson Space Center, Houston, Texas*

This design of the liquid-cooling garment for NASA spacesuits allows the suit to remove metabolic heat from the human body more effectively, thereby increasing comfort and performance while reducing system mass. The garment is also more flexible, with fewer restrictions on body motion, and more effectively transfers thermal energy from the crewmember's body to the external cool-

ing unit. This improves the garment's performance in terms of the maximum environment temperature in which it can keep a crewmember comfortable.

The garment uses flexible, highly thermally conductive sheet material (such as graphite), coupled with cooling water lines of improved thermal conductivity to transfer the thermal energy from the body to the liquid cooling lines

more effectively. The conductive sheets can be layered differently, depending upon the heat loads, in order to provide flexibility, exceptional in-plane heat transfer, and good through-plane heat transfer. A metal foil, most likely aluminum, can be put between the graphite sheets and the external heat source/sink in order to both maximize through-plane heat transfer at the con-



tact points, and to serve as a protection to the highly conductive sheets. Use of a wicking layer draws excess sweat away from the crewmember's skin and the use of an outer elastic fabric ensures good thermal contact of the highly conductive underlayers with the skin.

This allows the current state of the art to be improved by having cooling lines that can be more widely spaced to im-

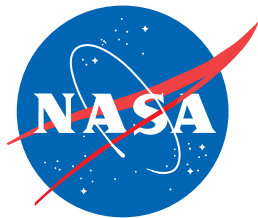
prove suit flexibility and to reduce weight. Also, cooling liquid does not have to be as cold to achieve the same level of cooling. Specific areas on the human body can easily be targeted for greater or lesser cooling to match human physiology; a warmer external environment can be tolerated, and spatial uniformity of the cooling garment can be improved to reduce vasoconstriction limits.

Elements of this innovation can be applied to other embodiments to provide effective heat transfer over a flexible and surface-conformable fashion without the limitation of fluid freeze points.

*This work was done by Warren P. Ruetemele, Grant C. Bue, and Evelyne Orndoff of Johnson Space Center and Henry Tang of Muniz Engineering. Further information is contained in a TSP (see page 1). MSC-24189-1*







National Aeronautics and  
Space Administration